

UNCLASSIFIED

AD NUMBER

AD016790

LIMITATION CHANGES

TO:

Approved for public release; distribution is unlimited.

FROM:

Distribution authorized to DoD only; Administrative/Operational Use; 01 JUN 1953. Other requests shall be referred to Office of Naval Research, ATTN: Code 280, 875 North Randolph Street, Arlington, VA 22203. Pre-dates formal DoD distribution statements. Treat as DoD only.

AUTHORITY

ONR ltr dtd 9 Nov 1977

THIS PAGE IS UNCLASSIFIED

AD 16790

Massachusetts Institute of Technology
Department of Electrical Engineering
Servomechanisms Laboratory

ELECTRONIC NUCLEAR INSTRUMENTATION GROUP

D.I.C. Project No. 6986

Technical Report No. 1

**DESIGN CRITERIA FOR LOW-LEVEL
SECOND-HARMONIC
MAGNETIC MODULATORS**

by

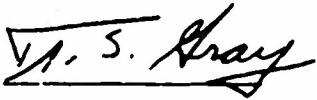
Earl Justin Kletsy

Office of Naval Research
Contract N5ori-07876
NR-025-164

Abstract: An analysis for the second-harmonic magnetic modulator used as a detector for low-level low-frequency signals is presented. This analysis, verified by experiment, is used to formulate design criteria for the modulator.

Consideration is given to factors influencing the choice of windings, excitation source frequency, and output frequency. Figures of merit for modulators and core materials are presented as well as considerations concerning core shape and size. Circuit configurations are discussed which relax output filter requirements. The relative merits of several circuit techniques used to realize maximum power gain are presented.

June 1, 1953

Approved: 

This report is based on a thesis having the same title submitted by the author in partial fulfillment of the requirements for the degree of Master of Science in Electrical Engineering at the Massachusetts Institute of Technology. The research described in this document was made possible through support extended the Massachusetts Institute of Technology by the Office of Naval Research and the Navy Bureau of Ships.

TABLE OF CONTENTS

	Page
TABLE OF SYMBOLS.....	111
CHAPTER I INTRODUCTION.....	1
CHAPTER II MATHEMATICAL ANALYSIS OF OPERATION.....	3
2.1 Principle of Operation.....	3
2.2 No-Signal Operation.....	5
2.3 Operation with Signal.....	9
2.4 Variation of Output with Amplitude of Excitation.....	11
2.5 Dynamical Characteristic (Time-Constant).....	14
2.6 Power Gain.....	15
2.7 Figure of Merit.....	19
2.8 Extension of Results to a Practical Two- Core Current-Excited Modulator.....	19
CHAPTER III EXPERIMENTAL RESULTS.....	23
3.1 Core Parameters.....	23
3.2 Output Voltage Curves.....	29
3.3 Power Gain Curves.....	36
CHAPTER IV CONCLUSIONS AND DESIGN CONSIDERATIONS.....	42
4.1 Choice of Modulator Configuration.....	42
4.2 Choice of Excitation.....	43
4.3 Choice of Output.....	44
4.4 Choice of Core.....	44
4.41 Core Material.....	44
4.42 Core Shape and Size.....	47

TABLE OF CONTENTS (continued)

	Page
4.5 Windings	47
4.6 Circuits for Realizing Maximum Power Gain...	48
CHAPTER V WORK SUGGESTED BY THE PRESENT STUDY.....	52
5.1 Behavior of Higher Output Harmonics.....	52
5.2 Threshold and Overload Signal Levels.....	52
5.3 Verification of μ_m/μ_a as a Figure of Merit for Core Materials.....	52
5.4 Voltage-Excited Modulator.....	53
5.5 Determination of Frequency Response.....	53
5.6 Power Measurement.....	53
ACKNOWLEDGMENT.....	54
BIBLIOGRAPHY	55

TABLE OF SYMBOLS

A	- core cross-section	(cm ²)
a	- voltage amplitude	(volts)
B	- flux density	(gauss)
B _s	- saturation flux density	(gauss)
E ₂	- peak value of 2nd-harmonic voltage	(volts)
e _o	- instantaneous value of output voltage	(volts)
F ₁	- modulator figure of merit	(sec ⁻¹)
G	- power gain	(dimensionless)
H	- magnetizing force	(oersteds)
H _c	- coercive force	(oersteds)
H _m	- peak value of excitation magnetizing force	(oersteds)
H _o	- magnetizing force produced by signal	(oersteds)
H _s	- saturation value of magnetizing force	(oersteds)
I _m	- peak value of excitation current	(amperes)
I _o	- signal current	(amperes)
I _s	- saturation value of excitation current	(amperes)
i _e	- instantaneous value of excitation current	(amperes)
i _{sig}	- instantaneous value of signal current	(amperes)
L	- signal winding inductance	(henries)
ℓ	- mean core length	(cm)
N _e	- number of turns in excitation winding	(turns)
N _o	- number of turns in output winding	(turns)
n	- order of harmonic component	(dimensionless)
P _{in}	- signal power input	(watts)

P_o	- useful power output	(watts)
R_L	- load resistance	(ohms)
R_w	- signal winding resistance	(ohms)
T	- period of excitation	(sec)
t	- general time variable	(sec)
t_d	- time delay due to hysteresis	(sec)
t_r	- rise time of trapezoidal excitation	(sec)
X_2	- impedance of output winding at 2nd-harmonic frequency	(ohms)
α	- slope of flux density	(gauss/sec)
δ	- width of output voltage pulses	(sec)
ϵ_A	- amplitude error	(volts)
ϵ_s	- slope error	(volts/sec)
μ_a	- average permeability of core	(gauss/oersted)
μ_m	- maximum permeability of core	(gauss/oersted)
τ	- time constant	(sec)
ϕ	- time delay due to signal	(sec)
γ	- slope of trapezoidal excitation	(oersted/sec)

CHAPTER I

INTRODUCTION

Major difficulties are encountered when d-c amplifiers are used to amplify low-level low-frequency signals. These difficulties are mainly problems of zero-drift and noise. One of the most successful techniques in circumventing the drift and noise problems is to convert the low-frequency intelligence to a frequency permitting conventional a-c amplification. The means for accomplishing the frequency conversion have been mainly mechanical--choppers, vibrating capacitors, and similar devices. These devices by their very nature, must be operated at relatively low sampling rates and are subject to the usual failures of moving equipment.

This paper presents an analysis and design criteria for the magnetic modulator. The modulator, as a frequency conversion device, offers solutions to the problems stated above. It converts low-level low-frequency signals into an amplitude-modulated suppressed-carrier output. The device has extremely low inherent zero-drift, wide dynamic range extending down to d-c, and considerable power gain. Along with these electrical characteristics, the modulator has no vacuum tubes, no moving parts, nor does it require critical adjustment; hence it is extremely rugged and practically maintenance free.

In spite of the modulator's desirable features, it has not found widespread application. A glance into the history of the magnetic modulator indicates why its striking characteristics have not been previously exploited, and what is needed to exploit these characteristics more fully.

The basic operating principle of the magnetic modulator has been known for many years. In the early twenties the Bell Telephone Laboratories carried out preliminary investigation of the modulator (Ref. 4). However, the lack of high permeability magnetic materials and the advent of a new and interesting device--the vacuum tube--caused research on the magnetic modulator to bog down and for the next 15 or 20 years the device lay dormant.

During World War II the modulator was re-examined, and with the aid of new magnetic materials, developed into an extremely sensitive air-borne magnetometer for use in submarine detection and geological survey (Ref. 5). Some basic analytic expressions for the characteristics of the modulator were formulated at that time but these are not of sufficient generality to be of use in the over-all design of magnetic modulators.

In 1950 Williams and Noble (Ref. 11) indicated that the fundamental limitation on signal level was the presence of Barkhausen noise inherent in the core material. This established the lowest detectable signal level at about 10^{-19} watts per cycle of bandwidth.

In 1951 Manley (Ref. 8), of the Bell Telephone Laboratories, set forth some expressions for output voltage, power gain, and rise-time; but once again the results do not readily lend themselves to design procedures.

Thus the need for a general analysis of the operation of the magnetic modulator is felt. The analysis presented here is the result of a combined physical, geometrical, and mathematical interpretation of modulator operation. Experimental work has been carried out to verify the analytic expressions. On the basis of the analytic and experimental work some general design considerations are discussed.

CHAPTER II

MATHEMATICAL ANALYSIS OF OPERATION

2.1 Principle of Operation

In its most general form, the magnetic modulator can be represented by the block diagram shown in Fig. 2.1. Notice that this device differs from an ordinary modulator in that the even harmonics of the excitation (carrier) are amplitude-modulated by the signal while the carrier itself is not. Any one of the even harmonics can be employed as the output or the summation of several or all even harmonics can be used.

In its simplest form, Fig. 2.2, the modulator consists of a single high-permeability toroid wound with a separate winding for excitation, signal, and output.

If the excitation current waveform has zero-axis symmetry, then the resulting core flux (and hence the voltage induced in the output winding) contains only fundamental and odd-harmonic components because of the odd-symmetrical character of the hysteresis loop of the core. If a d-c or modulating frequency signal is applied to the signal winding, even-harmonic components also appear in the output. For small values of signal there exists a linear relation between the signal and the amplitude of the even-harmonic components. The sense of the signal is preserved in the phase of the output with respect to the excitation.

The extremely low zero-drift of the modulator arises from the symmetrical character of the hysteresis loop around which the device operates. This symmetry is not disturbed by either temperature or frequency.

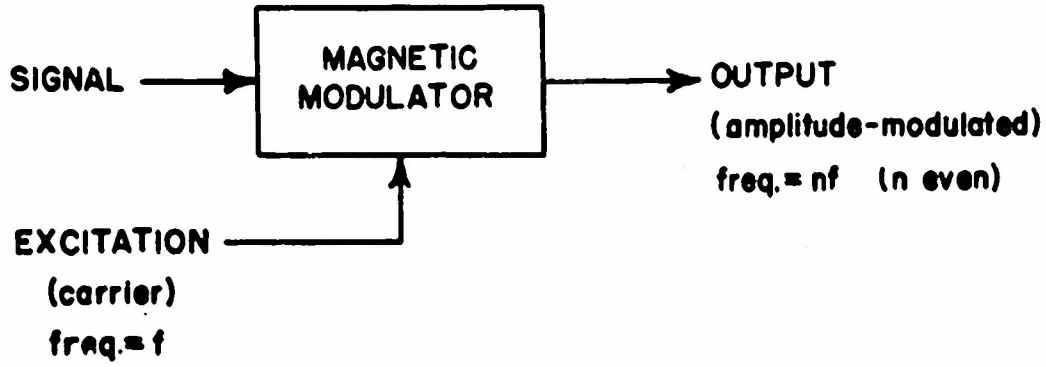


FIG. 2.1 General Magnetic Modulator

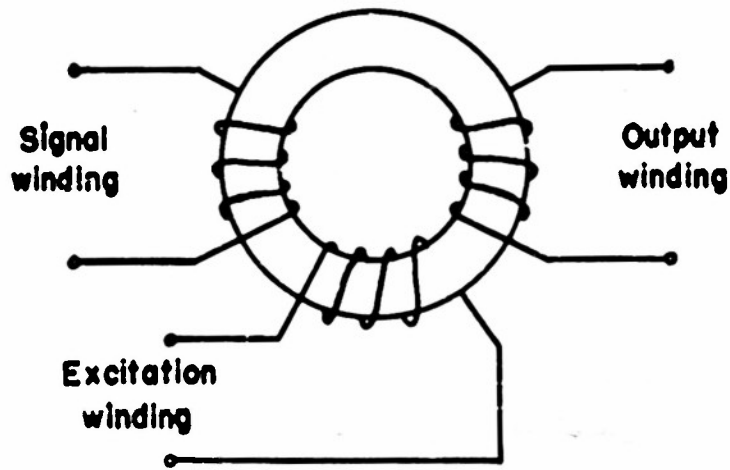


FIG. 2.2 Simple Magnetic Modulator

Separate windings may be used for excitation, signal, and output as shown in Fig. 2.2; or two or more functions may be served by a single winding thus allowing winding space to be used to best advantage.

There are many modes of operation of the modulator. Excitation and/or signal may be supplied from voltage or current sources or from sources of finite impedance. The output may be taken as a voltage or a current.

The analysis which follows treats the case where both signal and excitation sources are of high impedance and the output is taken as a voltage.

2.2 No-Signal Operation

The circuit to be analyzed is shown in Fig. 2.3. Functionally the output voltage is given by:

$$e_o(t) = -N_o A \frac{dB}{dt} = -N_o A \frac{d}{dt} [B(H)] \quad H = f(i_{sig}). \quad (1)$$

In order to set up useful mathematical relations for the operation of the modulator it is necessary to describe analytically the non-linear flux-current characteristic shown in Fig. 2.4(a). A reasonable piece-wise linear approximation; incorporating maximum permeability, finite saturation permeability, and hysteresis, is indicated in Fig. 2.4(b). Fig. 2.4(c), which assumes no saturation permeability, has been found adequate when the maximum permeability is high. If hysteresis is neglected the approximation of Fig. 2.4(d) results.

A geometrical interpretation of equation (1) using the simplest approximation to the flux-current characteristic is shown in Fig. 2.5.

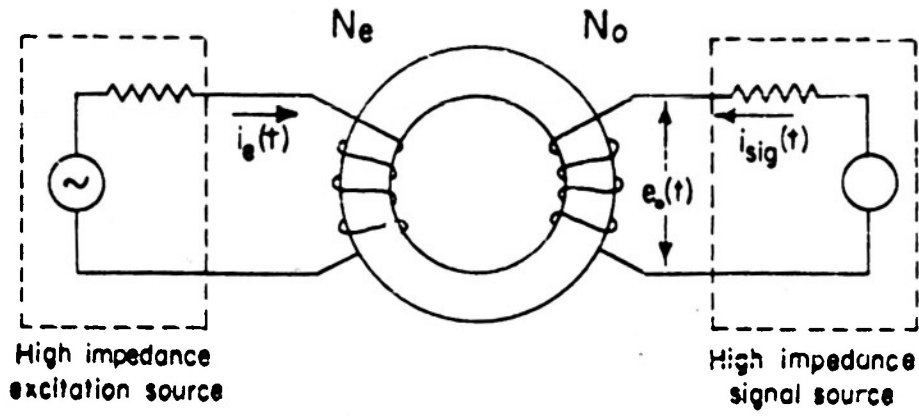


FIG. 2.3 High Impedance Modulator

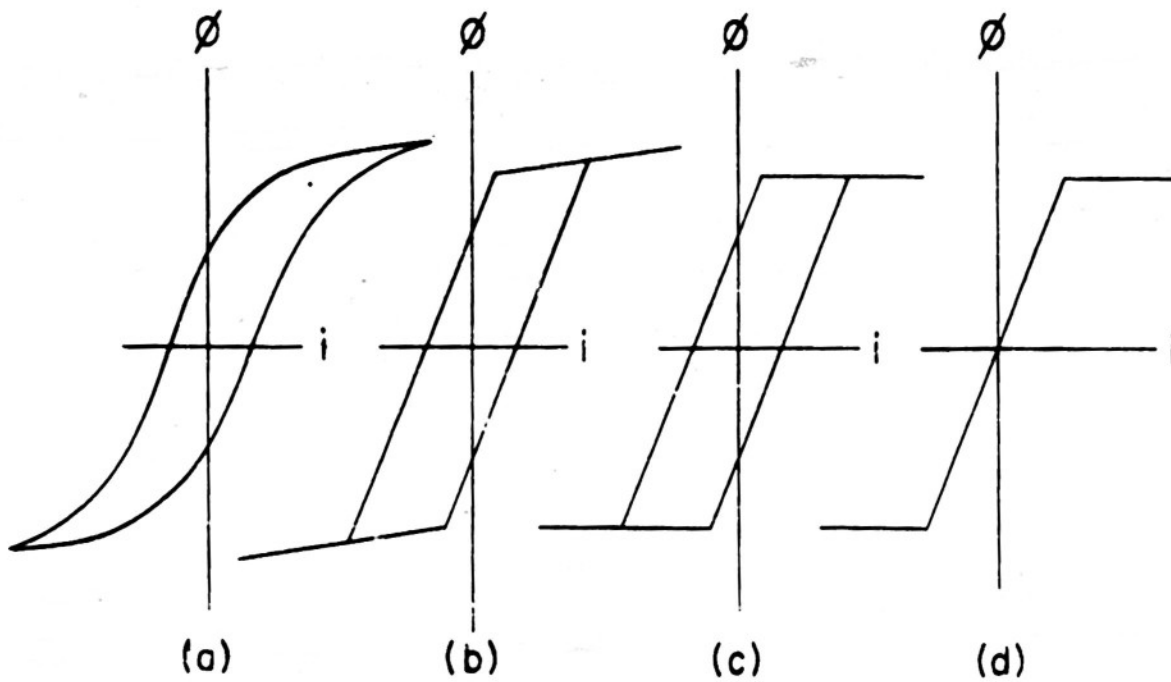


FIG. 2.4 Approximations to Flux-Current Characteristic

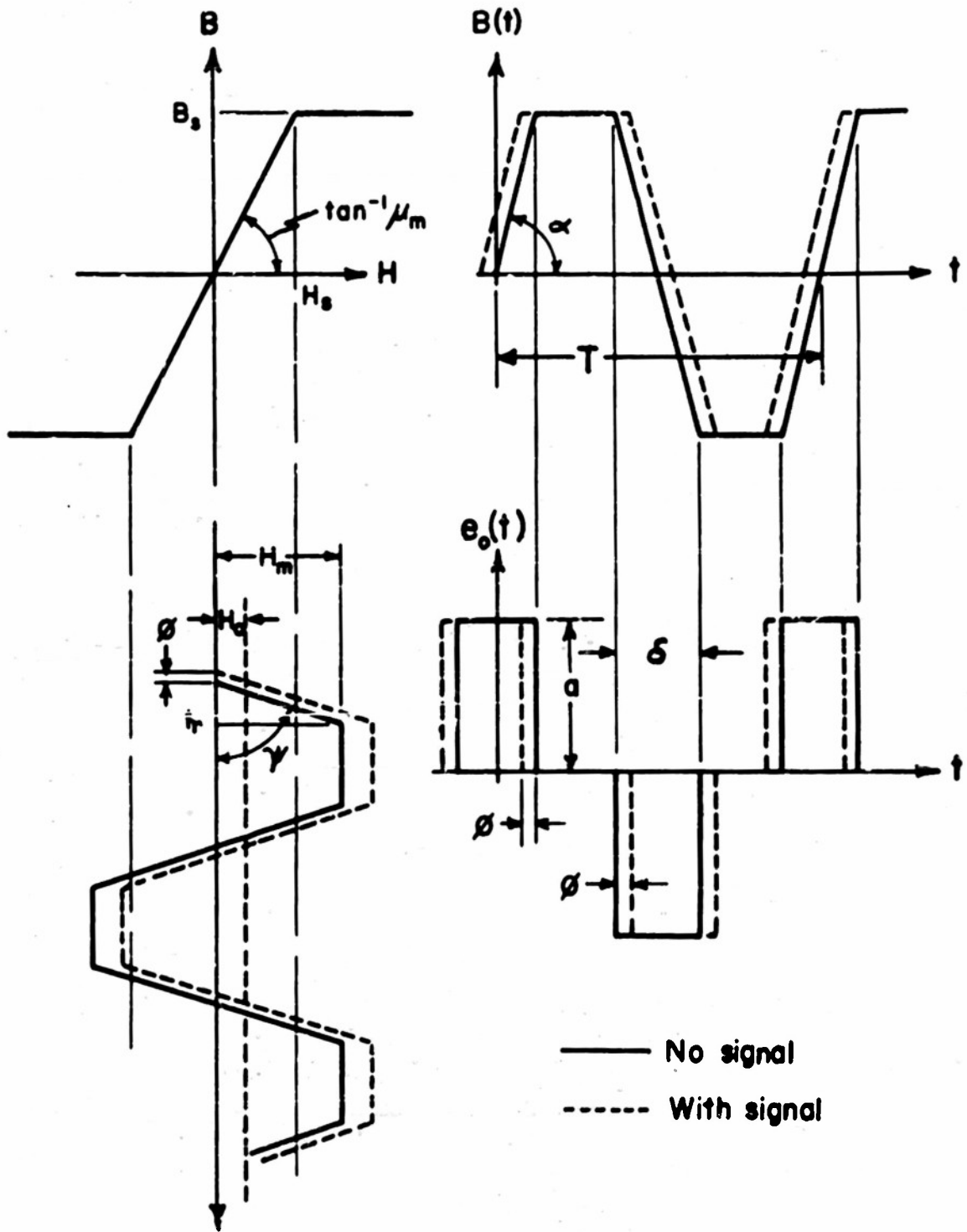


FIG.2.5 Geometrical Interpretation of Modulator Operation

Sinusoidal excitation current can be approximated by the trapezoid shown for simplicity in the analysis. The validity of this approximation is borne out experimentally; its maximum error will be shown analytically in section 2.4.

Fig. 2.5 indicates that if the excitation current is trapezoidal, the flux is also a trapezoidal function of time. The output voltage, found from the time derivative of the flux, consists of rectangular pulses.

A Fourier Series expansion of the output voltage will yield its harmonic components. Consider the output to consist of the sum of a set of positive pulses and a similar set of negative pulses shifted π radians. These sets are given respectively by:

$$f_+(t) = \frac{a\delta}{T} + \sum_{n=1}^{\infty} \frac{2a}{n\pi} \sin \frac{n\pi\delta}{T} \cos \frac{2n\pi t}{T} \quad (2)$$

$$f_-(t) = -\frac{a\delta}{T} - \sum_{n=1}^{\infty} \frac{2a}{n\pi} \sin \frac{n\pi\delta}{T} \cos \left(\frac{2n\pi t}{T} + n\pi \right). \quad (3)$$

The output voltage is therefore:

$$e_o(t) = f_+(t) + f_-(t) = \sum_{n=1}^{\infty} \frac{2a}{n\pi} \sin \left(\frac{n\pi\delta}{T} \right) \left[\cos \left(\frac{2n\pi t}{T} \right) - \cos \left(\frac{2n\pi t}{T} + n\pi \right) \right]. \quad (4)$$

Using the fact that $\cos(x + y) = \cos x \cos y - \sin x \sin y$, equation (4) reduces to:

$$e_o(t) = \sum_{n=1}^{\infty} \frac{2a}{n\pi} \left[1 - (-1)^n \right] \sin \frac{n\pi\delta}{T} \cos \frac{2n\pi t}{T}. \quad (5)$$

Note that $e_o(t)$ contains only odd harmonics since when n is even $[1 - (-1)^n]$ is zero.

2.3 Operation with Signal

When a signal I_0 (corresponding to a magnetizing force equal to H_0) is applied, the dotted lines in Fig. 2.5 indicate the manner in which the output is altered. With signal, the positive set of pulses is advanced by amount ϕ radians and the negative set retarded by the same amount. The Fourier Series for these sets are given respectively by:

$$f_+(t) = \frac{a\delta}{T} + \sum_{n=1}^{\infty} \frac{2a}{n\pi} \sin \frac{n\pi\delta}{T} \cos \left(\frac{2n\pi t}{T} + n\phi \right) \quad (6)$$

$$f_-(t) = -\frac{a\delta}{T} - \sum_{n=1}^{\infty} \frac{2a}{n\pi} \sin \frac{n\pi\delta}{T} \cos \left(\frac{2n\pi t}{T} + n\pi - n\phi \right). \quad (7)$$

The output voltage is:

$$e_o(t) = f_+(t) + f_-(t) = \sum_{n=1}^{\infty} \frac{2a}{n\pi} \sin \left(\frac{n\pi\delta}{T} \right) \left[\cos \left(\frac{2n\pi t}{T} + n\phi \right) - \cos \left(\frac{2n\pi t}{T} + n\pi - n\phi \right) \right]. \quad (8)$$

Applying the trigonometric identity used above, equation (8) reduces to:

$$e_o(t) = \sum_{n=1}^{\infty} \frac{2a}{n\pi} \sin \frac{n\pi\delta}{T} \left\{ \left[1 - (-1)^n \right] \cos n\phi \cos \frac{2n\pi t}{T} - \left[1 + (-1)^n \right] \sin n\phi \sin \frac{2n\pi t}{T} \right\}. \quad (9)$$

The geometrical parameters a , δ , and ϕ of equation (9) can be replaced by electrical equivalents derived from the geometry of Fig. 2.5:

$$\tan \alpha = \mu_m \tan \psi = \mu_m \frac{H_m}{I_r} \quad (10)$$

$$\delta = 2 \text{ (time required for excitation to reach } H_s) \quad (11a)$$

$$\delta = 2 \frac{H_s}{\tan \psi} = 2 \frac{H_s t}{H_m} \quad (11b)$$

$$a = -N_o A \times 10^{-8} \frac{dB}{dt} = -N_o A \mu_m \frac{H_m}{t_r} \times 10^{-8} \quad (12)$$

$$\phi = \frac{H_o}{\tan \psi} = \frac{t_r H_o}{H_m} \text{ (sec.)} = \frac{2\pi t_r H_o}{T H_m} \text{ (rad.)} . \quad (13)$$

Making the substitutions indicated, equation (9) yields, for n odd:

$$e_o(t) = - \sum_{n \text{ odd}}^{\infty} \frac{4 N_o A \mu_m H_m}{n\pi t_r} \sin\left(\frac{2n\pi t_r}{T} \frac{H_o}{H_m}\right) \cos\left(\frac{2n\pi t_r}{T} \frac{H_o}{H_m}\right) \cos \frac{2n\pi t}{T} \quad (14)$$

and for n even:

$$e_o(t) = - \sum_{n \text{ even}}^{\infty} \frac{4 N_o A \mu_m H_m}{n\pi t_r} \sin\left(\frac{2n\pi t_r}{T} \frac{H_o}{H_m}\right) \sin\left(\frac{2n\pi t_r}{T} \frac{H_o}{H_m}\right) \sin \frac{2n\pi t}{T} . \quad (15)$$

Under ordinary operating conditions $H_o \ll H_m$, thus:

$$\cos\left(\frac{2n\pi t_r}{T} \frac{H_o}{H_m}\right) \rightarrow 1 \quad \text{and} \quad \sin\left(\frac{2n\pi t_r}{T} \frac{H_o}{H_m}\right) \rightarrow \frac{2n\pi t_r}{T} \frac{H_o}{H_m} .$$

Under these conditions equations (14) and (15) reduce respectively to:

$$e_o(t) = - \sum_{n \text{ odd}}^{\infty} \frac{4 N_o A \mu_m H_m}{n\pi t_r} \sin\left(\frac{2n\pi t_r}{T} \frac{H_o}{H_m}\right) \cos \frac{2n\pi t}{T} \quad (16)$$

$$e_o(t) = - \sum_{n \text{ even}}^{\infty} 8 N_o A \mu_m f H_o \times 10^{-8} \sin\left(\frac{2n\pi t_r}{T} \frac{H_o}{H_m}\right) \sin \frac{2n\pi t}{T} . \quad (17)$$

Thus, with the assumption that the signal be small, equation (17) shows that the amplitudes of the even harmonic components of the output voltage are linearly related to the signal.

In most applications, only the second-harmonic component is used as an output. This is done for two reasons.

- 1) Simple narrow-band amplification can be used.
- 2) The impedance level of the source of the second-harmonic is lower than that of any higher harmonic source.

For the second-harmonic, equation (17) becomes:

$$\begin{aligned}
 e_2(t) &= \left[-8 N_0 \Lambda \mu_m f H_0 \times 10^{-8} \sin \left(4\pi f \frac{H_s}{H_m} t_r \right) \right] \sin 4\pi f t \\
 &= \left[-3.2 \pi N_0^2 \frac{\Lambda}{\lambda} \mu_m f I_0 \times 10^{-8} \sin \left(4\pi f \frac{H_s}{H_m} t_r \right) \right] \sin 4\pi f t . \quad (18)
 \end{aligned}$$

2.4 Variation of Output with Amplitude of Excitation

Equations (17) and (18) indicate that the output voltage is a function of the amplitude and rise-time of the excitation as well as a function of the signal. Therefore, an optimum excitation signal is indicated. Its characteristics are found by setting

$$\sin 4\pi f \frac{H_s}{H_m} t_r = \pm 1 \quad \text{or} \quad 4\pi f \frac{H_s}{H_m} t_r = \frac{\pi}{2} .$$

Thus:

$$\frac{H_s}{t_r} = 8H_0 f = \tan \psi . \quad (19)$$

Equation (19) indicates the optimum slope of the excitation waveform in the unsaturated region.

If the excitation waveform is sinusoidal and given by:

$$H(t) = H_m \sin 2\pi f t, \quad (20)$$

then its initial slope is:

$$\left. \frac{dH}{dt} \right|_{t=0} = 2\pi f H_m \cos 2\pi f t \Big|_{t=0} = 2\pi f H_m = \tan \psi . \quad (21)$$

If this value of slope is assumed to be constant in the unsaturated region, then the optimum amplitude of excitation can be found by equating equations (19) and (21):

$$\tan \psi = 8H_s f = 2\pi f H_m \quad \therefore \frac{H_m}{H_s} = \frac{4}{\pi} . \quad (22)$$

The variation of output voltage (for fixed signal) under the above assumption is found by introducing equation (21) into equation (18). This yields, neglecting the minus sign:

$$\frac{E_2}{8 N_o A \mu_m f H_o \times 10^{-8}} = \sin 2 \frac{H_s}{H_m} \quad (23)$$

A normalized plot of this variation is shown in Fig. 2.6. The approximation to the magnetic characteristic accounts for the discontinuity in the curve at $\frac{H_m}{H_s} = 1$.

An analysis based directly on a sinusoidal excitation waveform (Ref. 5) yields the dotted curve shown in Fig. 2.6.

The validity of the trapezoidal approximation is shown graphically in Fig. 2.6 and its maximum errors are indicated by the following argument.

Consider the trapezoidal approximation to a sinusoid with the amplitude adjusted to give maximum output according to equation (22) as shown in Fig. 2.7. The only region of interest is between $H = 0$ and $H = H_s$ since once saturation occurs the excitation waveform is immaterial.

The maximum error in amplitude occurs at $\theta = .785$ radians. This error is:

$$E_A = .785 - \sin .785 = .785 - .705 = .08 \approx 11\% . \quad (24)$$

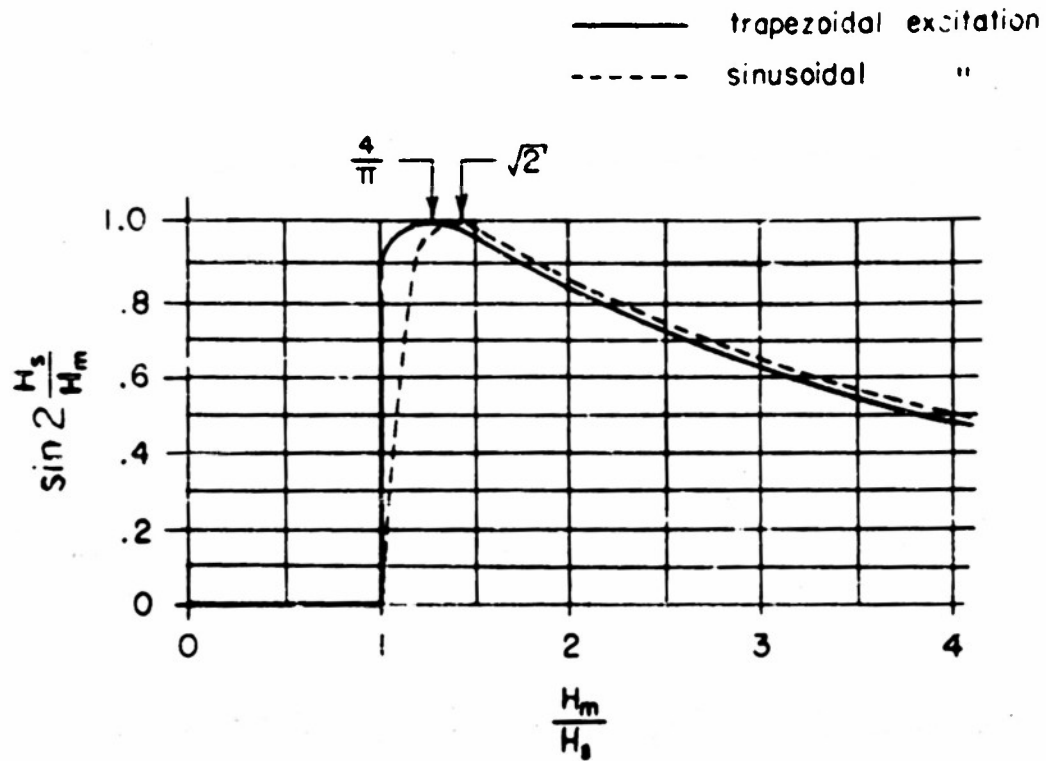


FIG.2.6 Variation of Output Voltage with Excitation Amplitude

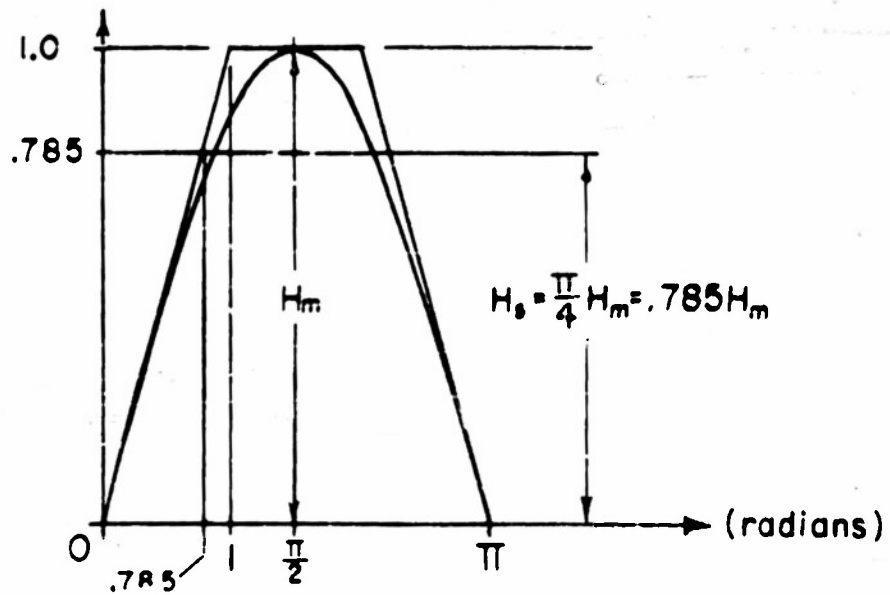


FIG.2.7 Comparison between Sinusoidal & Trapezoidal Approximations

The maximum error in slope occurs at $\sin \theta = .735$. This error is:

$$\epsilon_s = 1 - \cos \left(\sin^{-1} .735 \right) = 1 - .615 = .385 \approx 40\% \quad (25)$$

These quantities represent maximum instantaneous values of error. When H_m is increased, the difference between sinusoid and trapezoid decreases in the region of interest. Values of H_m less than $\frac{4}{\pi} H_s$ are not used since the output decreases rapidly as shown in Fig. 2.6. Experimental results indicate the errors ϵ_a and ϵ_s are not significant.

2.5 Dynamical Characteristic (Time-Constant)

The dynamic response of the modulator and its associated output filter is a function of the dynamic characteristics of both the signal input winding and the output filter. The design of the output filter depends on the application of the modulator and its dynamic characteristics can normally be synthesized to give any reasonable response. Since the output filter can be designed to give better dynamic response than the signal input winding, the dynamic behavior of the modulator is determined by a single parameter--the time-constant of the signal input winding.

In so far as signal is concerned, the signal input winding consists of an inductance L in series with the d-c winding resistance R_w . Thus the winding time-constant is given by:

$$\tau = \frac{L}{R_w} \quad (26)$$

The inductance of the signal winding can be calculated as follows:

$$L \frac{di}{dt} = N \frac{d\phi}{dt} \cdot 10^{-8} \quad \phi = B A \quad H = \frac{4\pi N I}{10 \ell} \quad (27)$$

$$L = \frac{N_o \phi}{I} 10^{-8} = \frac{N_o B A}{H(10\lambda)} 4\pi N_o = \frac{N_o^2 \mu_a A}{\lambda} \frac{4\pi}{10} \times 10^{-8}. \quad (28)$$

An average value of $\mu = \mu_a$, corresponding to the slope of the magnetization curve is used in the calculation of inductance, rather than the maximum value μ_m .

Combining equations (26) and (28), the winding time constant becomes:

$$\tau = \frac{L}{R_w} = 4\pi \frac{N_o^2 \mu_a A}{\lambda R_w} \times 10^{-9}. \quad (29)$$

Important in a system using phase-sensitive demodulation is the time delay caused by hysteresis. As a first approximation this delay is a constant depending only on the shape of the hysteresis loop. Fig. 2.8 indicates the time delay graphically when an idealized hysteresis loop and trapezoidal excitation are considered. The amount of time delay t_d is given by:

$$t_d = \frac{H_c}{\tan \gamma} = \frac{H_c}{H_m} t_r. \quad (30)$$

For the case of sinusoidal excitation (see equations 19, 20 and 21):

$$\frac{H_m}{t_r} = 2\pi f H_m. \quad \therefore \frac{t_d}{T} = \frac{1}{2\pi} \frac{H_c}{H_m}. \quad (31)$$

2.6 Power Gain

It has been found experimentally that for high-impedance excitation a reasonable Thevenin equivalent for the modulator as seen by the load consists of a voltage source in series with an inductor as shown in Fig. 2.9. The voltage source E_2 is equal to the open-circuit

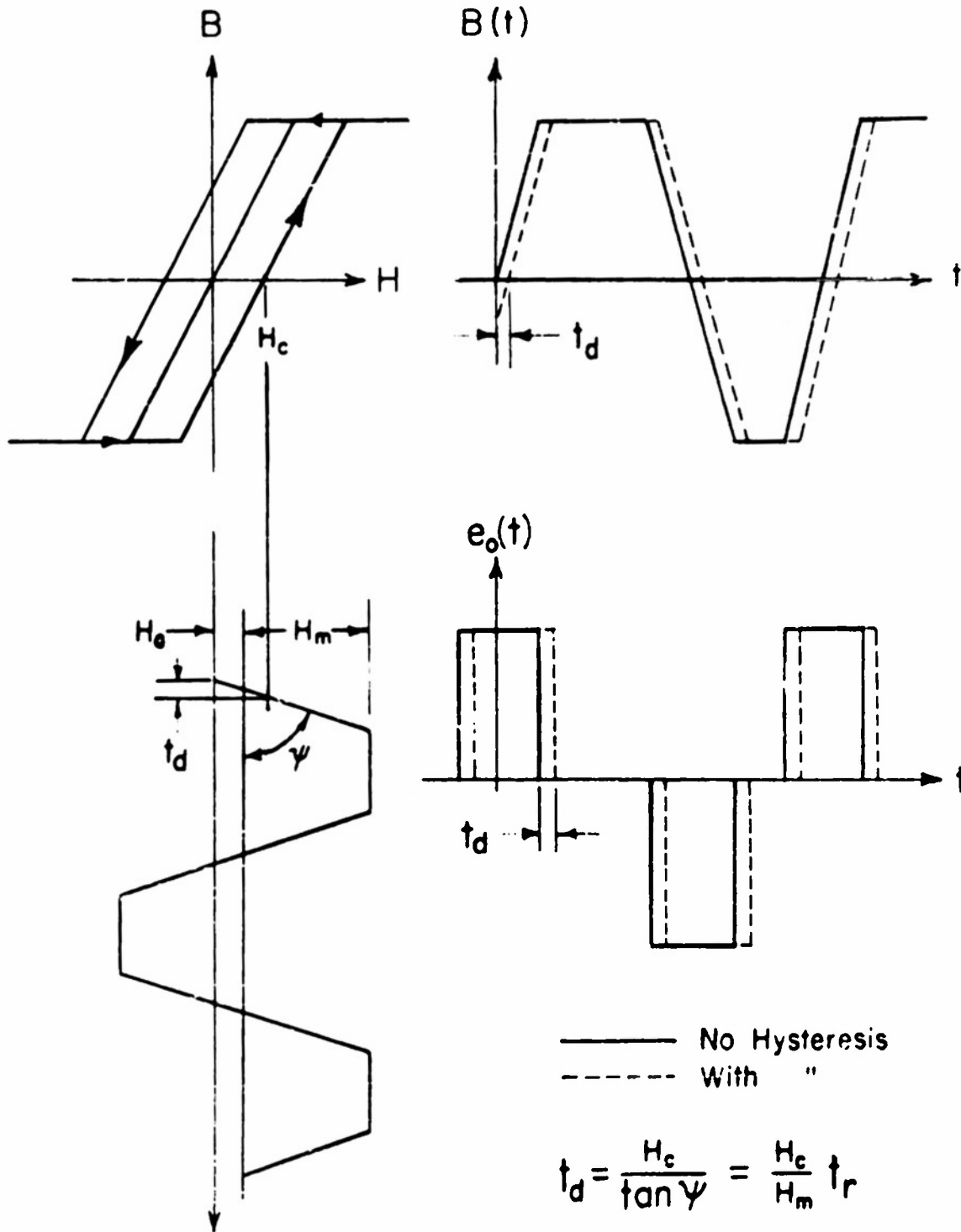


FIG.2.8 Approximation to Time-Delay Produced by Hysteresis

second-harmonic voltage calculated from equation (18). X_2 is equal to the reactance of the output winding inductance evaluated at the second-harmonic frequency.

Elementary circuit theory indicates that maximum power transfer to the load occurs when R_L equals the magnitude of X_2 . (It is assumed that $R_w \ll 2\omega L$).

Thus the power delivered to R_L is:

$$P_o = \frac{\left(\frac{E_2}{\sqrt{2}}\right)^2}{R_L} = \frac{\left(\frac{E_2}{\sqrt{2}}\right)^2}{|X_2|} = \frac{\left(-8 N_o A \mu_m f H_o \times 10^{-8}\right)^2}{2(2\omega L)} = \frac{\left(-32\pi^2 \frac{A}{\lambda} \mu_m f I_o \times 10^{-9}\right)^2}{8\pi f L}$$

$$= \frac{128\pi^4 \mu_m^2 \frac{A^2}{\lambda^2} I_o^2 f \times 10^{-18}}{L} = 3.2N_o^2 \frac{A}{\lambda} \frac{\mu_m^2}{\mu_a} I_o^2 f \times 10^{-8}. \quad (32)$$

The signal power dissipated in the signal winding is:

$$P_{in} = I_o^2 R_w. \quad (33)$$

Maximum power gain is therefore:

$$G_{max} = \frac{P_o}{P_{in}} = \frac{3.2N_o^2 \frac{A}{\lambda} \frac{\mu_m^2}{\mu_a} I_o^2 f \times 10^{-8}}{I_o^2 R_w} = \frac{8}{\pi} \frac{L}{R_w} \left(\frac{\mu_m}{\mu_a}\right)^2 f. \quad (34)$$

If the signal winding is used for both signal and output as in Fig. 2.10, then the power gain expression must be modified to include the signal power lost in R_L . The signal power delivered by the signal source is:

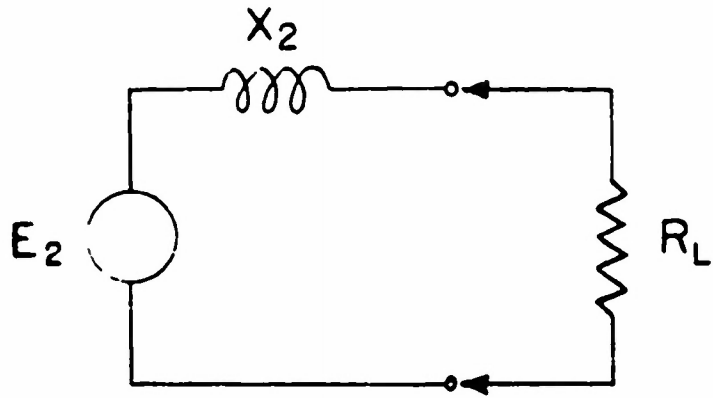


FIG.2.9 Thevenin Equivalent for Output Winding as Seen by Load

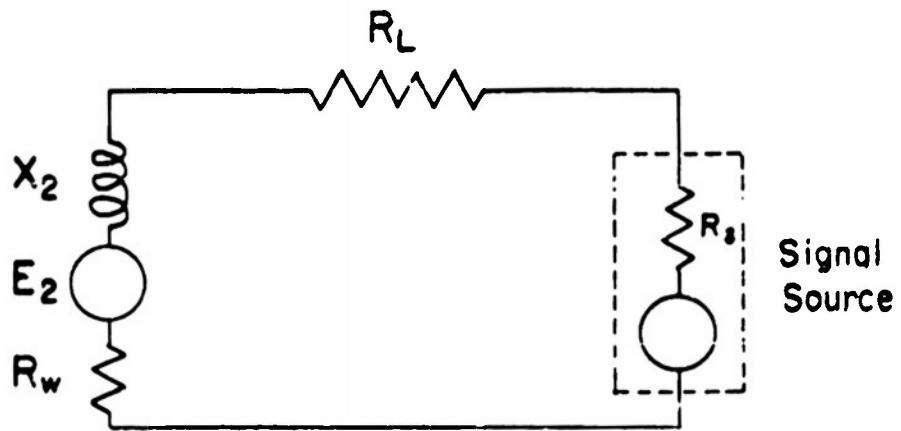


FIG.2.10 Equivalent Circuit for Modulator Employing Single Winding for Signal & Output

$$P_{in} = I_0^2 (R_w + R_L) . \quad (33a)$$

The maximum power gain is now:

$$G_{max} = \frac{g}{\pi} \frac{L}{R_w + R_L} \left(\frac{\mu_m}{\mu_a} \right)^2 f . \quad (34a)$$

2.7 Figure of Merit

Equation (34) can be rewritten in a form which expresses a figure of merit, F_1 , for modulator operation.

$$F_1 = \frac{\text{Power Gain}}{\text{Time Constant}} = \frac{G}{T} = \frac{g}{\pi} \left(\frac{\mu_m}{\mu_a} \right)^2 f . \quad (35)$$

While equation (35) does not account for hysteresis, core loss, or stray effects, it does indicate a fundamental design criterion for the modulator.

The factor $\frac{\mu_m}{\mu_a}$ occurs since the permeability upon which the output voltage depends differs from the value used to calculate nominal inductance. If experimental evidence indicates that this is actually the case, the factor $\frac{\mu_m}{\mu_a}$ can be considered as a figure of merit for core materials. In any event, for a given core material, the modulator figure of merit, F_1 , depends only on the frequency of operation.

2.8 Extension of Results to a Practical Two-Core Current-Excited Modulator

If two identical single-core modulators are arranged so that their excitation windings are in series and their output windings opposing, the combination doubles the even-harmonic output components and reduces

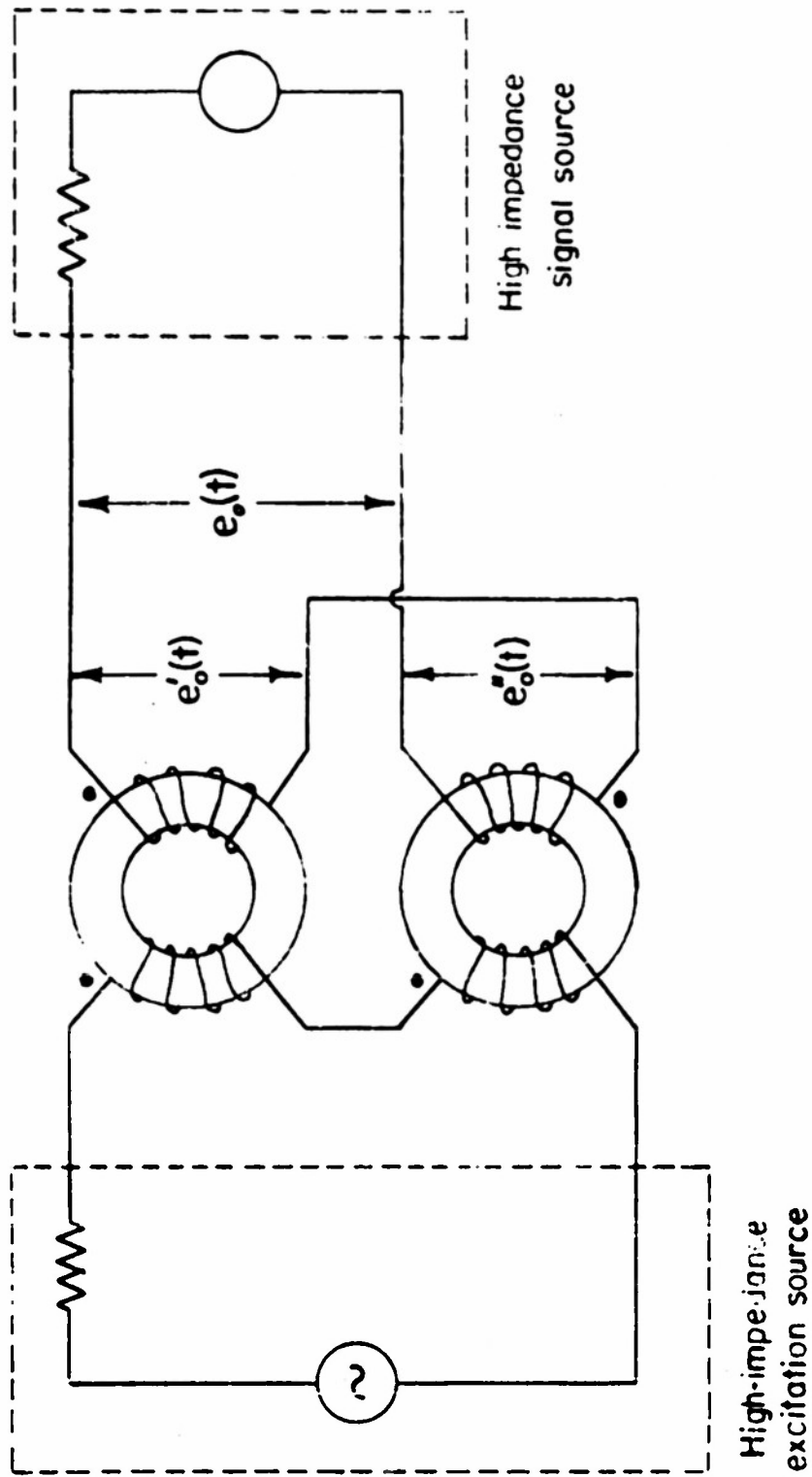


FIG. 2.11: 2-Core Current-Excited Modulator

the odd-harmonic output components to zero. Fig. 2.11 shows such an arrangement.

Reference to equations (14) and (15) indicates that the odd-harmonics vary as $\cos 2n\pi ft$ while the even-harmonics vary as $\sin 2n\pi ft$. The output voltage in Fig. 2.10 is given by:

$$e_o(t) = e_o'(t) + e_o''(t) . \quad (36)$$

For odd harmonics:

$$e_o(t) = (\text{constant}) \left[\cos 2n\pi ft + \cos (2n\pi ft + n\pi) \right] = 0 . \quad (37)$$

For even harmonics:

$$e_o(t) = (\text{constant}) \left[\sin 2n\pi ft + \sin (2n\pi ft + n\pi) \right] = 2 (\text{constant}) \sin 2n\pi ft . \quad (38)$$

Expressions governing the operation of the 2-core current-excited modulator are now easily derived from the previous work:

Voltage output =

$$e_o(t) = \left[- 16 N_o \mu_m f H_o \times 10^{-8} \sin \left(4\pi f \frac{H_o}{H_m} t_r \right) \right] \sin 4\pi ft \quad (39a)$$

$$e_o(t) = \left[- 6.4\pi N_o^2 \mu_m f \frac{A}{l} I_o \times 10^{-8} \sin \left(2 \frac{H_o}{H_m} \right) \right] \sin 4\pi ft . \quad (39b)$$

$$\text{Time Constant} = \tau = \frac{2L}{2R_w} = 4\pi \frac{N_o^2 \mu_a A}{l R_w} \times 10^{-9} . \quad (40)$$

$$\text{Power Output} = P_o = \frac{\left(\frac{2E_2}{\sqrt{2}} \right)^2}{2R_L} = 6.4 N_o^2 \frac{A}{l} \frac{\mu_m^2}{\mu_a} I_o^2 f \times 10^{-8} . \quad (41)$$

$$\text{Power Gain} = G_{\max} = \frac{P_o}{I_o^2 (2R_w)} = \frac{8}{\pi} \frac{L}{R_w} \left(\frac{\mu_m}{\mu_a} \right)^2 f . \quad (42)$$

$$\text{Figure of Merit} = F_1 = \frac{8}{\pi} \left(\frac{L_m}{L_a} \right)^2 f . \quad (43)$$

Comparison of equations (29) and (40), (34) and (42), and (35) and (43) indicates that the time-constant, power gain, and figure of merit are the same for both one-core and two-core modulators. Thus, the only advantage of using a two-core modulator is the suppression of odd-harmonic components.

CHAPTER III
EXPERIMENTAL RESULTS

3.1 Core Parameters

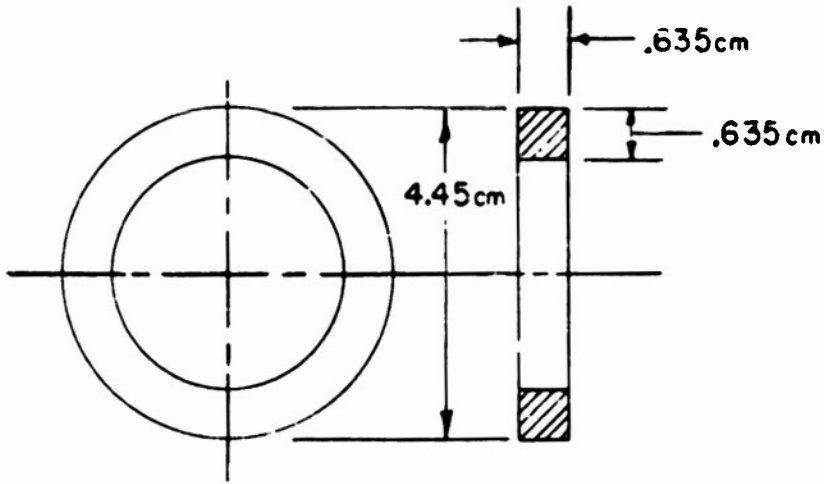
The experimental cores used were two 4-79 Mo-Permalloy toroids manufactured by the Arnold Engineering Company of Marengo, Illinois (Ref. 1). The toroids are tape-wound of 1-mil tape and enclosed in a nylon container to prevent depreciation of magnetic properties either by handling or wire winding. The physical dimensions of the cores are shown in Fig. 3.1.

Each core was wound with two 100-turn windings of No. 28 AWG enameled copper wire. For convenience in handling, the two cores were mounted on a discarded octal tube-base with each coil end brought out to a separate pin on the base. The completed experimental unit is pictured in Fig. 3.2.

The d-c resistance was measured with a laboratory Wheatstone Bridge and found to be 0.72 ohms per 100-turn winding.

The self-inductance was measured with a General Radio 650-A Impedance Bridge. The value obtained depends considerably on the amplitude of the bridge signal. The values ranged from 50 to 100 millihenries per 100-turn winding.

Magnetic characteristics of the core were determined with the aid of the circuit shown in Fig. 3.3 which allows the hysteresis loop to be displayed on the face of an oscilloscope.



cross sectional area = $A = 0.4 \text{ cm}^2$
mean length = $\lambda = 3.81\pi \text{ cm}$

FIG. 3.1 Physical Dimensions of Core

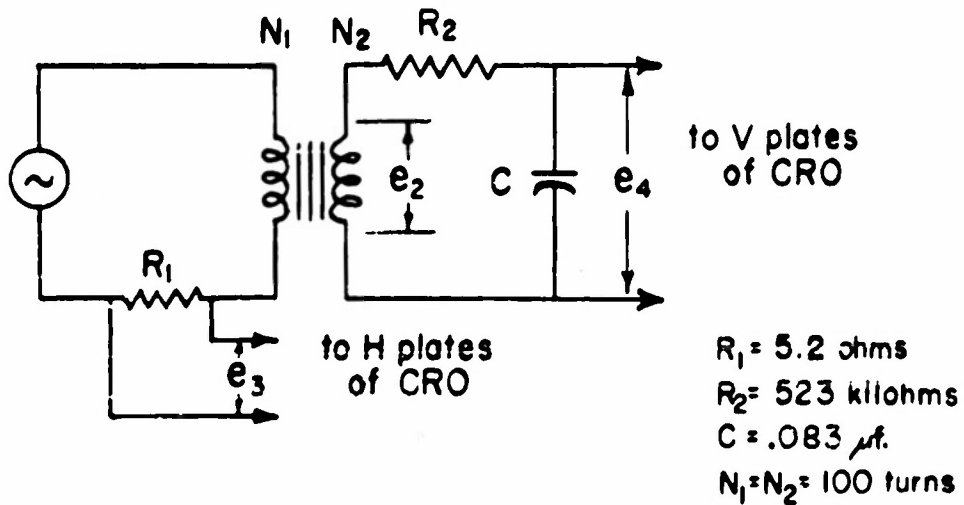


FIG. 3.3 Circuit Used to Plot Hysteresis Loops



FIG. 3.2 Mounted Experimental Unit

The loop can be calibrated by making use of the following relations:

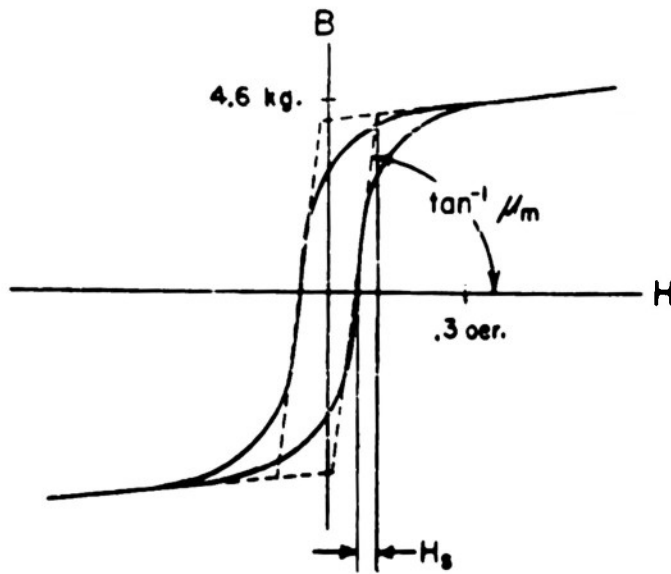
$$\begin{aligned} \phi_4 &\approx \frac{1}{RC} \int \phi_2 dt & \phi_2 &= N_2 \frac{d\phi}{dt} \times 10^{-8} \\ \phi &= \left(\frac{R_2 C}{N_2} 10^8 \right) \phi_4 & B &= \left(\frac{R_2 C}{N_2 A} 10^8 \right) \phi_4 \\ i &= \frac{\phi_3}{R_1} & H &= \frac{4\pi N_1 i}{10 l} \end{aligned} \quad (44)$$

The maximum permeability, μ_m , was found by recording the hysteresis loop at the frequency of interest and graphically measuring its maximum slope as shown in Fig. 3.4. The value of the saturation value of mmf, H_s , was then computed as the increment in mmf required to change the flux from zero to its saturation value.

The average value of permeability, μ_a , was assumed to be the slope of the normal magnetization curve. This curve, Fig. 3.5, was determined by plotting the tips of the hysteresis loops as the excitation increased. A straight line approximation was made and μ_a determined from the average slope in the unsaturated region.

The above experimental techniques yield the following results:

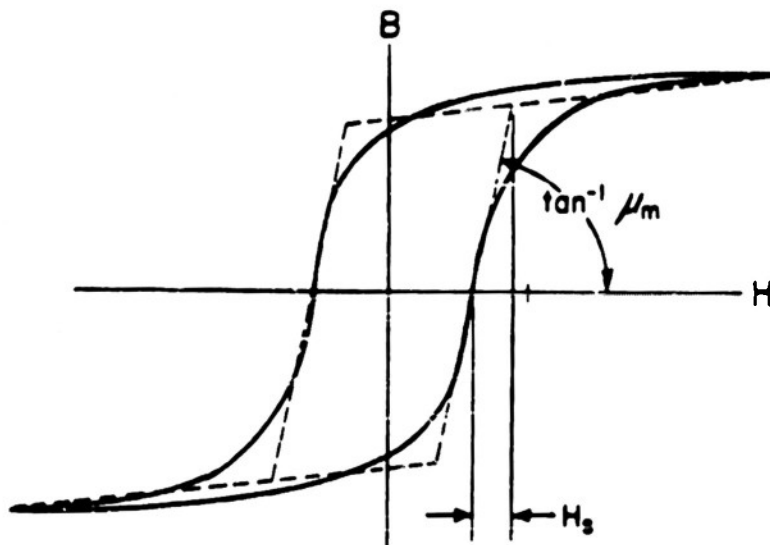
<u>600 cps</u>	<u>6000 cps</u>
$\mu_m = 10 \times 10^4$ gauss/oersted	$\mu_m = 5.3 \times 10^4$ gauss/oersted
$\mu_a = 4 \times 10^4$ gauss/oersted	$\mu_a = 2.6 \times 10^4$ gauss/oersted
$H_s = 0.042$ oersted	$H_s = 0.08$ oersted
$I_s = \frac{10 l}{4\pi N_1} H_s = 4.0$ ma.	$I_s = \frac{10 l}{4\pi N_1} H_s = 7.6$ ma.



600 cps loop

$\mu_m = 10 \times 10^4$ gauss/oersted

$H_s = 0.042$ oersted



6000 cps loop

$\mu_m = 5.3 \times 10^4$ gauss/oersted

$H_s = 0.08$ oersted

FIG. 3.4 Determination of Maximum Permeability μ_m

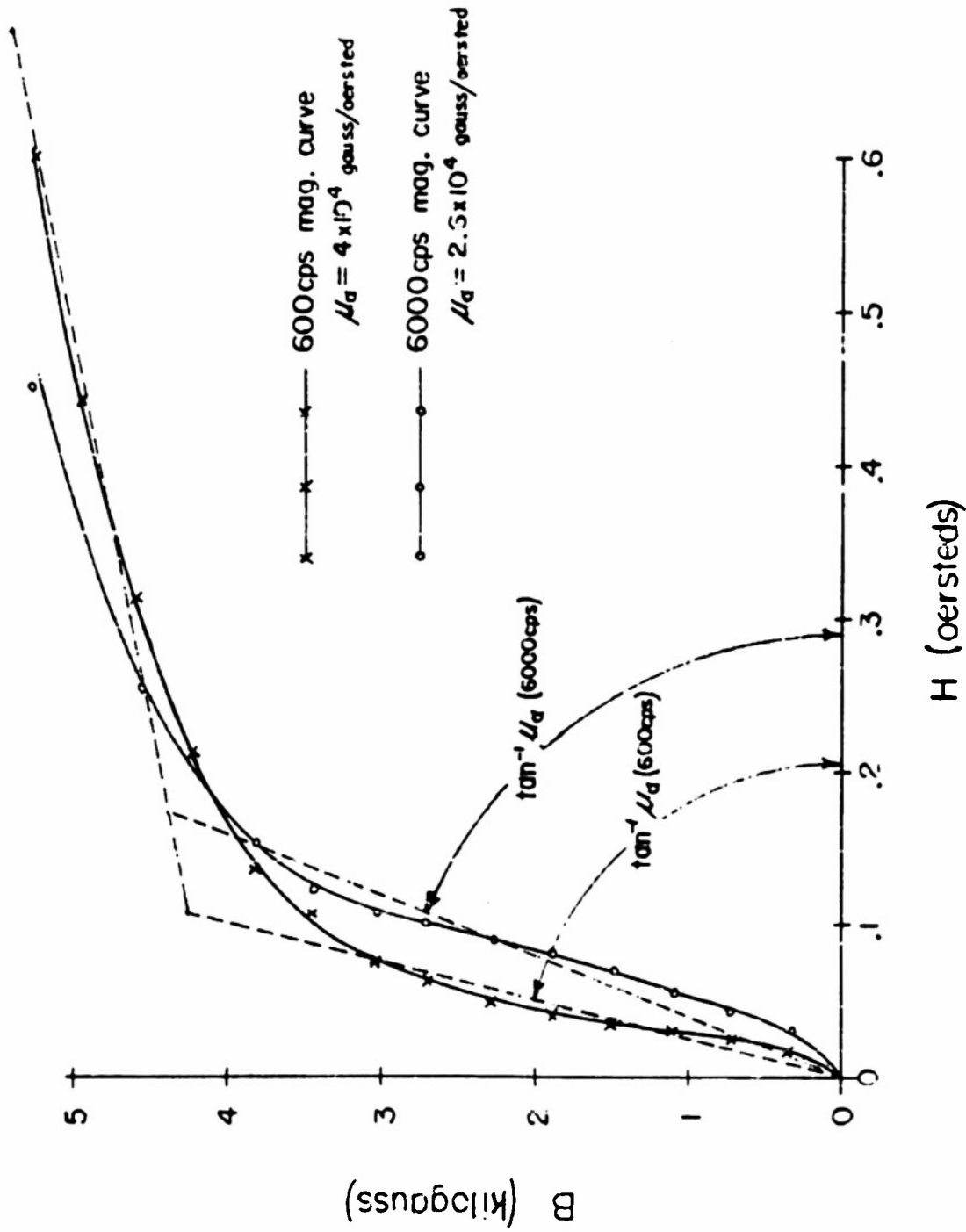


FIG. 3.5 Determination of Average Permeability μ_a

3.2 Output Voltage Curves

The 2-core current-excited modulator, Fig. 3.6, was chosen for experimental work because of its inherent rejection of odd-harmonics and its relatively larger voltage output. The indicated dot-markings refer to fundamental components of voltage.

Experimental curves of output voltage vs. excitation amplitude with fixed signal and output voltage vs. signal with fixed excitation are shown in Fig. 3.7 and 3.8 respectively. These curves were determined using the basic experimental circuit shown in Fig. 3.6. The output vs. signal curve is a cross-section of the output vs. excitation curve taken at the indicated values of excitation.

Excitation frequencies of 600 and 6000 cps were chosen to give reasonably large output signals and to be free of laboratory noise at the power frequency and its harmonics.

The curves shown in Fig. 3.7 can be normalized with respect to their peak amplitudes and also with respect to H_g . This is done for the case $I_0 = 100 \mu\text{a.}$ and the results compared to the predicted theoretical behavior (equation 23) in Fig. 3.9. If consideration is given to the difficulties encountered in measuring the magnetic parameters of the cores and to the approximations made for the hysteresis loop, the expressions of Chapter II are in fair agreement with these experimental results.

The expression for output voltage (equation 39b) becomes, upon substitution of the magnetic and physical parameters of the experimental cores,

$$\begin{aligned} e_o(t) &= \left[-6.73 \times 10^{-5} \mu_m I_0^2 \sin 2 \frac{H_g}{H_m} \right] \sin 4\pi ft & (45) \\ &= E_2 \sin 4\pi ft . \end{aligned}$$

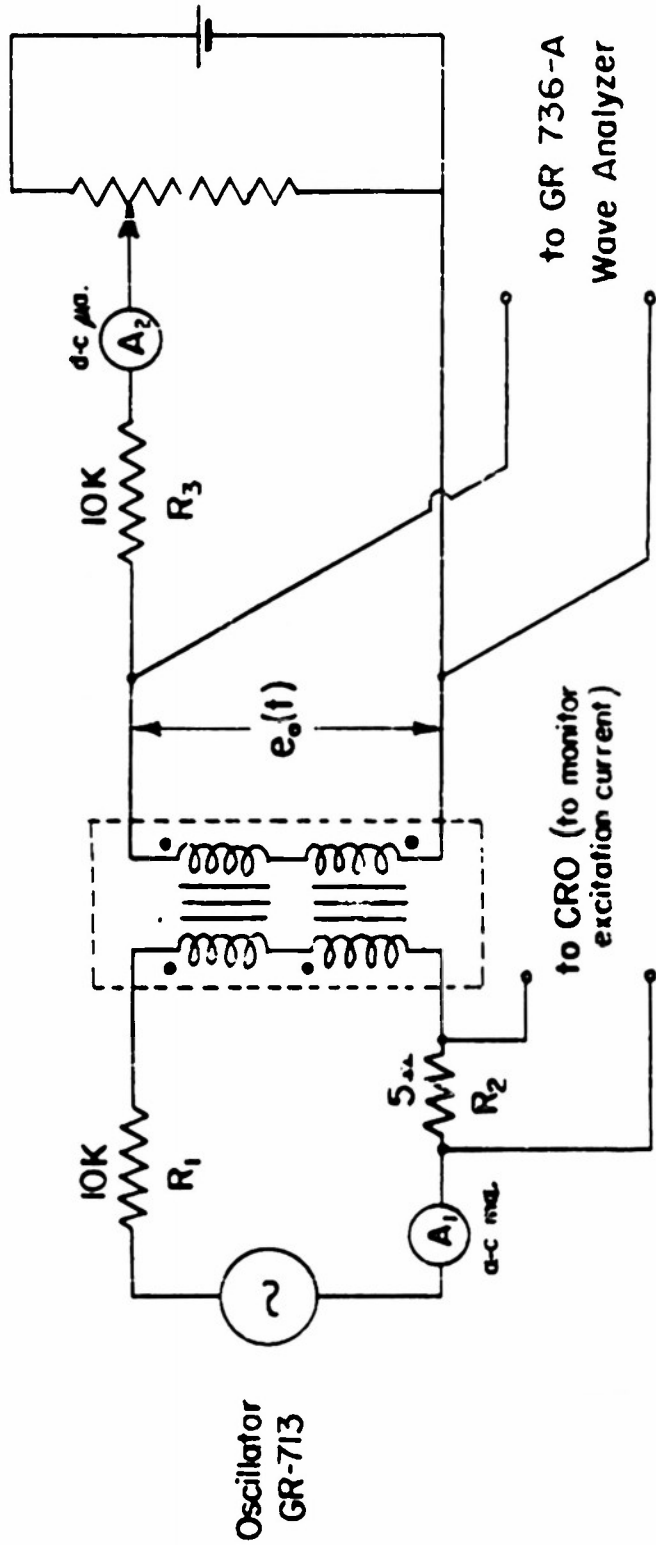


FIG. 3.6 Basic Experimental Circuit

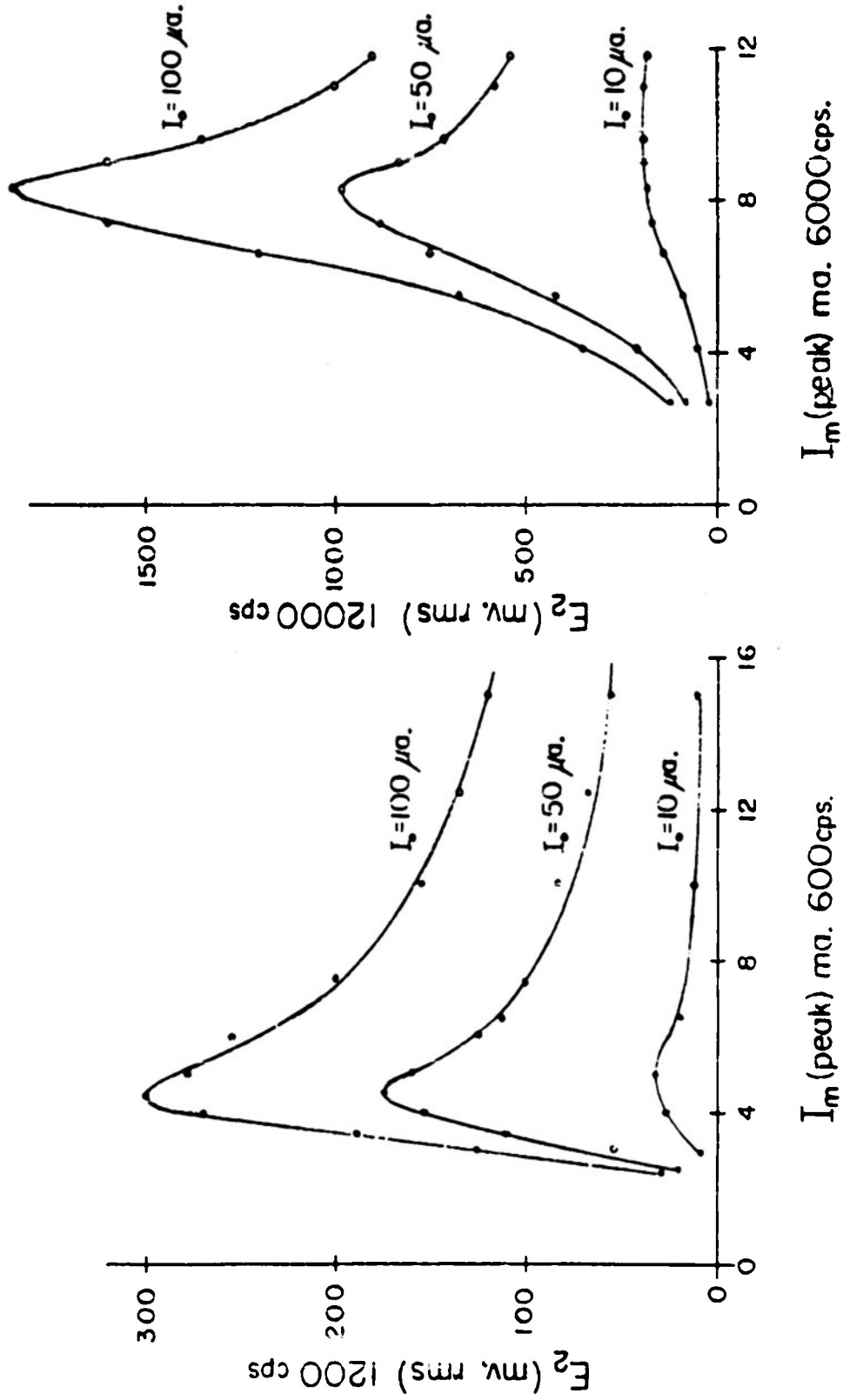


FIG. 3.7 Output Voltage vs. Excitation Amplitude

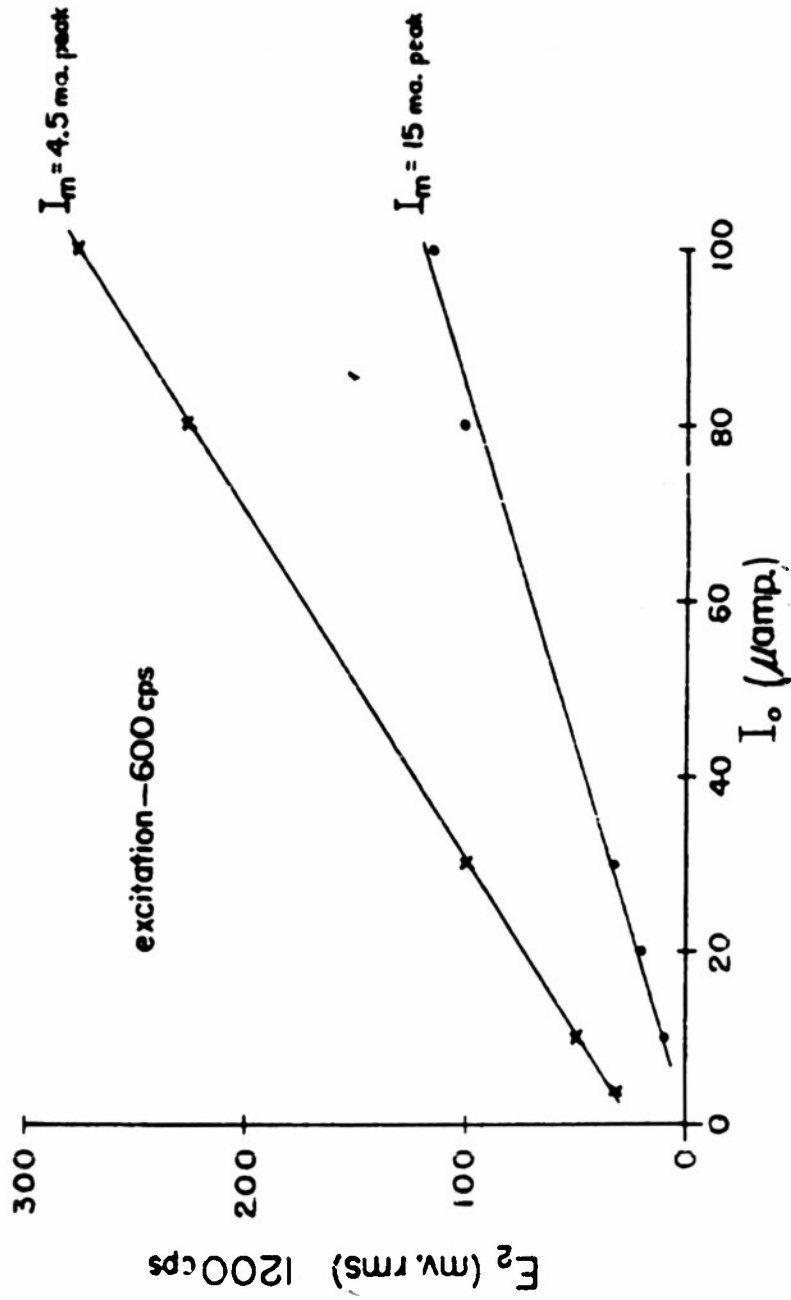


FIG. 3.8 Output Voltage vs. Signal

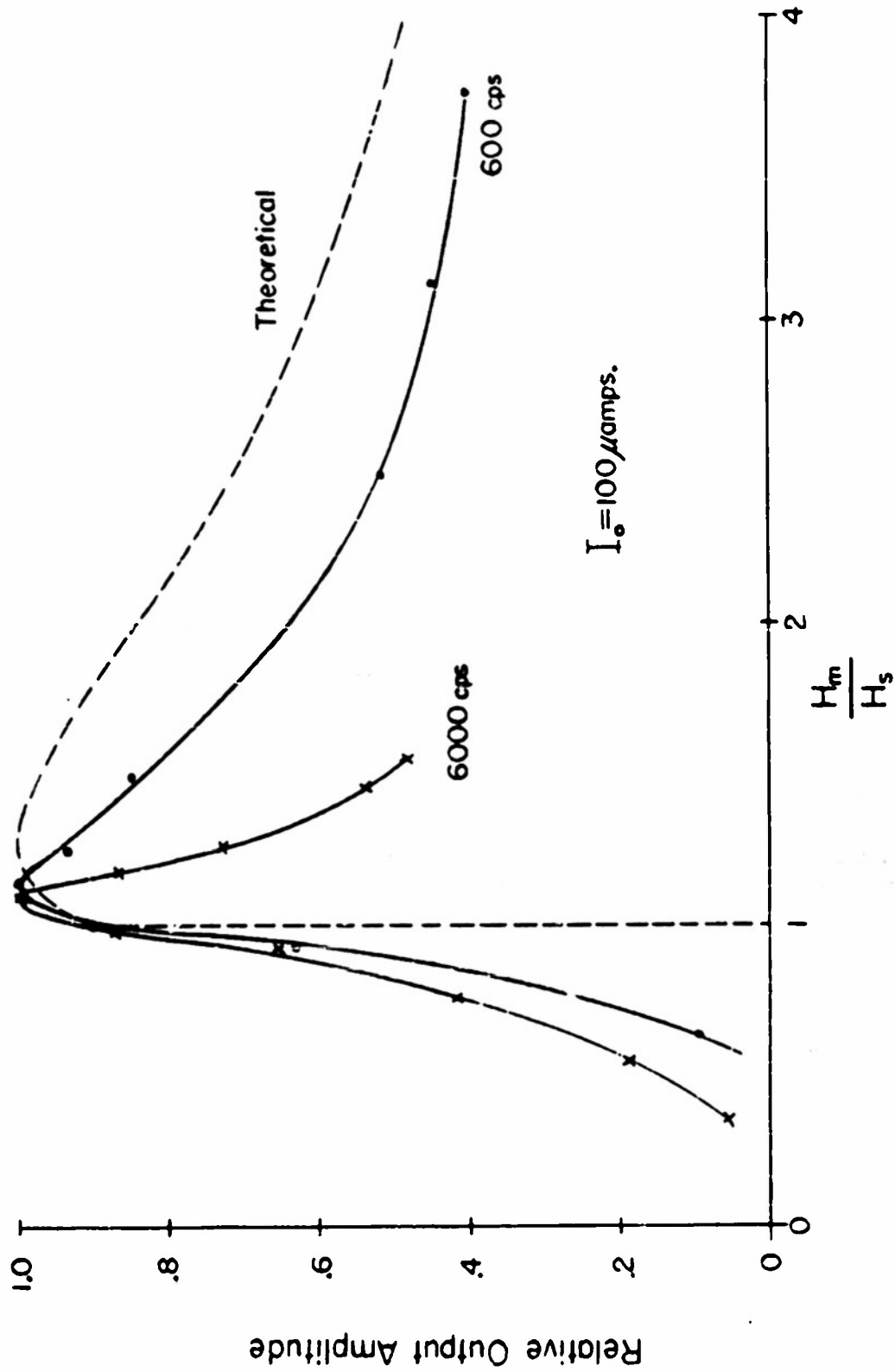


FIG. 3.9 Comparison of Excitation Amplitude Curves

For operation at 600 cps, $\mu_m = 10 \times 10^4$ and $H_g = 0.042$ oersted ($I_g = 4.0$ ma). Under these conditions the "transimpedance" becomes:

$$\frac{|E_2|}{I_0} = 6.73 \times 10^{-5} \times 10 \times 10^4 \times 600 \sin 2\left(\frac{4}{I_m}\right) = 4040 \sin 2\left(\frac{4}{I_m}\right). \quad (46)$$

Equation (46) is an expression for the slope of the curve shown in Fig. 3.8. A comparison of these quantities is shown below.

	E_2/I_0 (Eq. 46)	E_2/I_0 (Fig. 3.8)
$I_m = 4.5$ ma. (600 cps)	3940 ohms	3620 ohms
$I_m = 15$ ma. (600 cps)	2040 ohms	1830 ohms

In order to determine the effect of excitation frequency on transimpedance, the basic experimental circuit was used to obtain data for Fig. 3.10. At each point the amplitude of excitation current was adjusted to give maximum output voltage. Under these conditions the transimpedance is theoretically given by:

$$\frac{|E_2|}{I_0} = 6.73 \times 10^{-5} \mu_m f. \quad (47)$$

When applying equation (47), it is important to note that μ_m is a frequency dependent quantity. Shown on Fig. 3.10 are theoretical variations of transimpedance with frequency extrapolated from values of μ_m determined at 600 cps and 6000 cps.

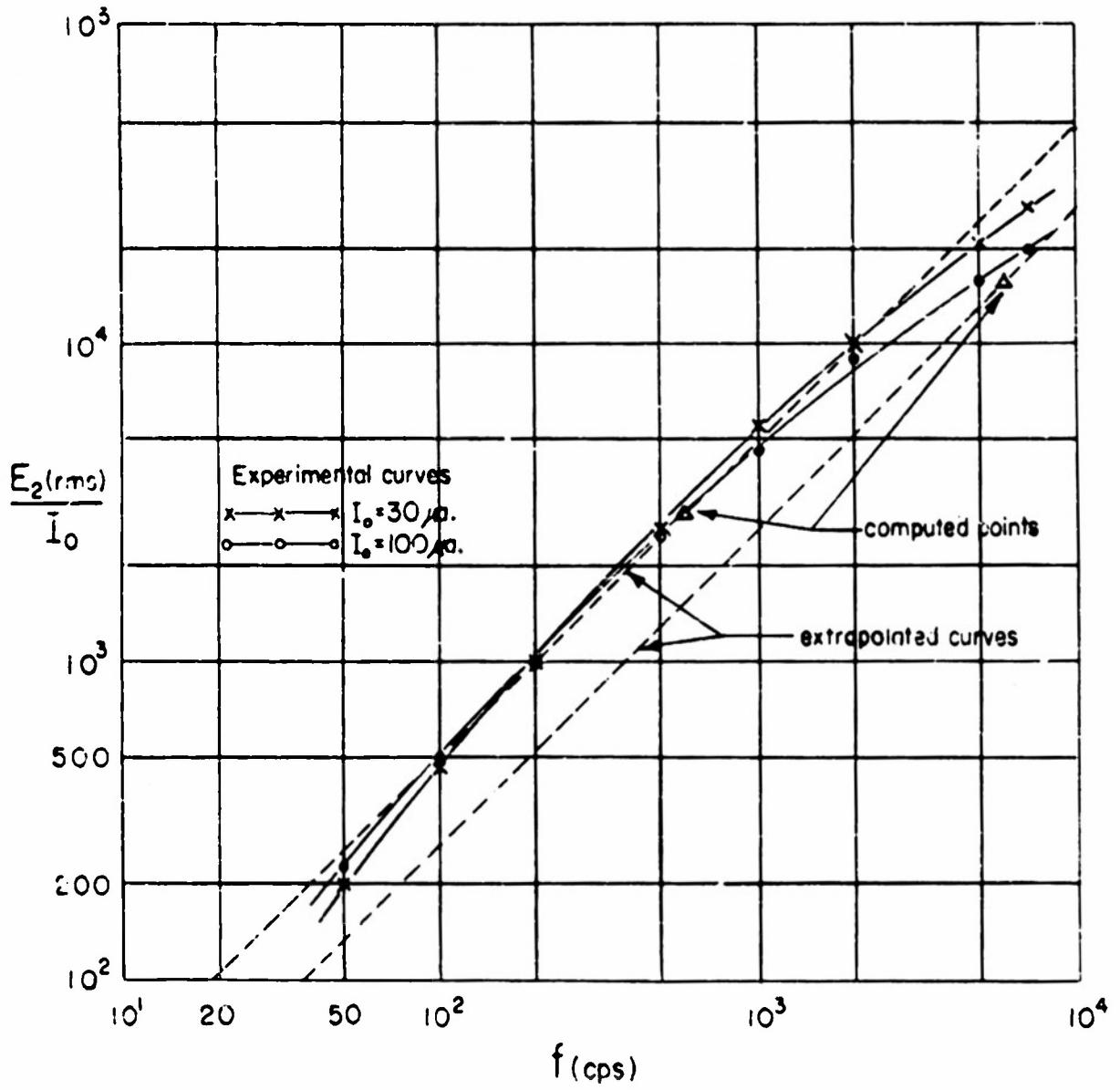


FIG. 3.10 Transimpedance vs. Frequency

3.3 Power Gain Curves

Power gain measurements were made using the circuit shown in Fig. 3.11. The somewhat elaborate scheme for measuring I_0 was necessary to eliminate the need for using a d-c microammeter of high resistance in series with the load R_L . The effective internal resistance of the signal source was about 0.1 ohm. This was achieved by using a 4 in. length of No. 32 AWG enameled copper wire for R_1 . Using this circuit it was possible, for each value of R_L , to adjust the signal current, I_0 , to the required fixed value without encountering meter loading.

Power output was measured by determining the second-harmonic component of the voltage appearing across R_L . This voltage squared and divided by R_L was considered to be power output. Power input was defined as the $I_0^2 R_w$ power developed in the modulator signal windings.

Measurements, for signals of 100 μ a., 30 μ a., and 10 μ a., were taken over five decades of resistance (R_L). The magnitude of the excitation current was adjusted to give maximum output voltage. Experimental results are indicated in Fig. 3.12. The variations from a smooth curve are caused by the inability to accurately set I_0 because of insufficient galvanometer sensitivity. If the results are averaged, and experimental error taken into account, a smooth curve can be drawn.

The nature of the effective source impedance at the second-harmonic frequency can be found by comparing the shape of the normalized power output curve with theoretical power transfer curves for pure resistive and pure reactive sources. This is done in Fig. 3.13. For this experimental case, it is apparent that a reasonable equivalent circuit for the modulator as seen by the load consists of a second-harmonic voltage source in series with a pure reactance.

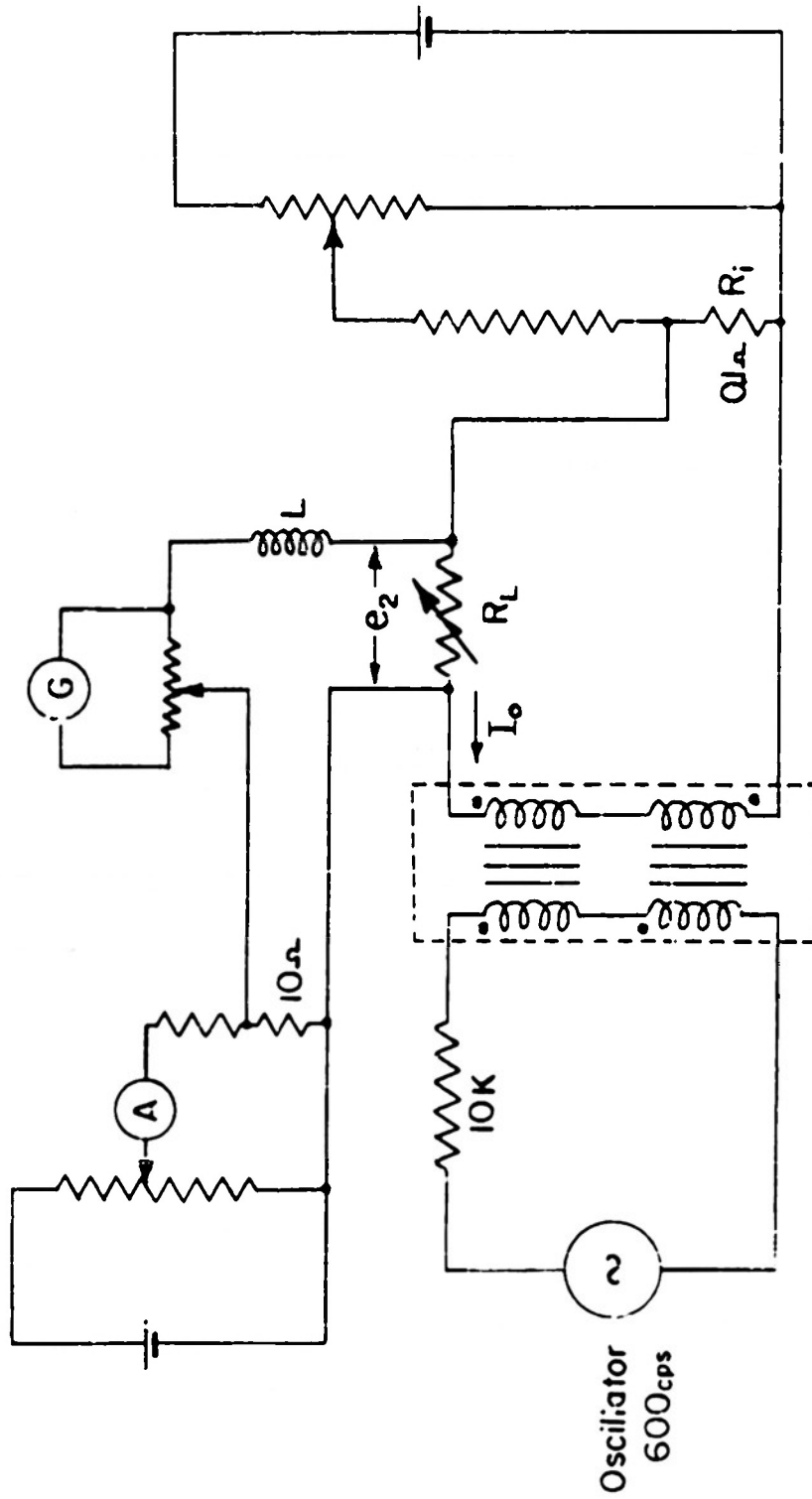


FIG. 3.11 Circuit for Power Gain Measurements

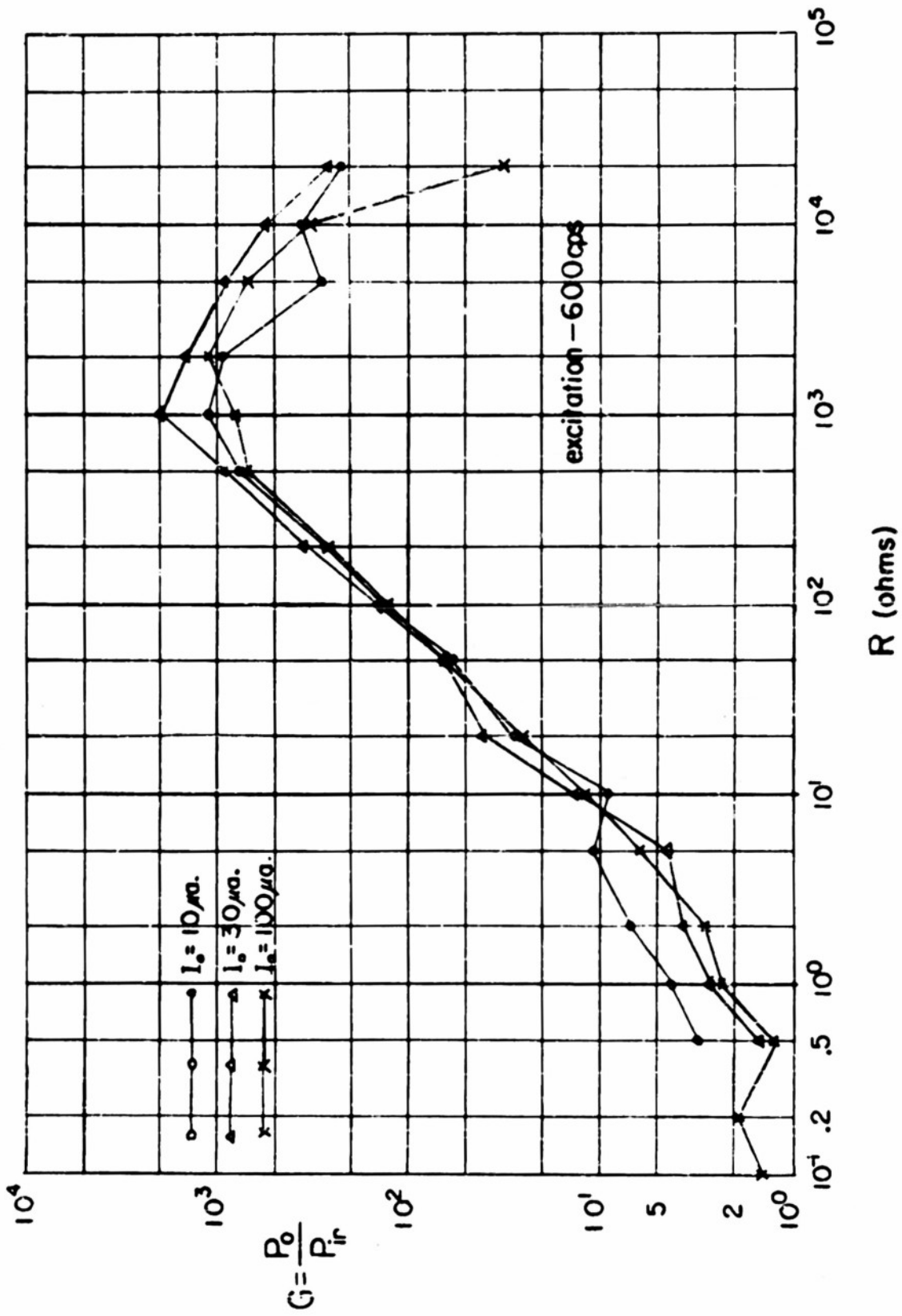
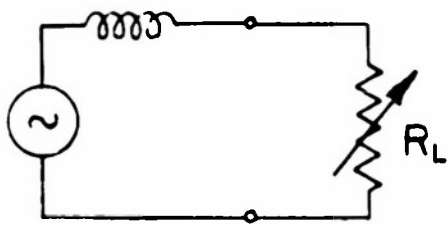
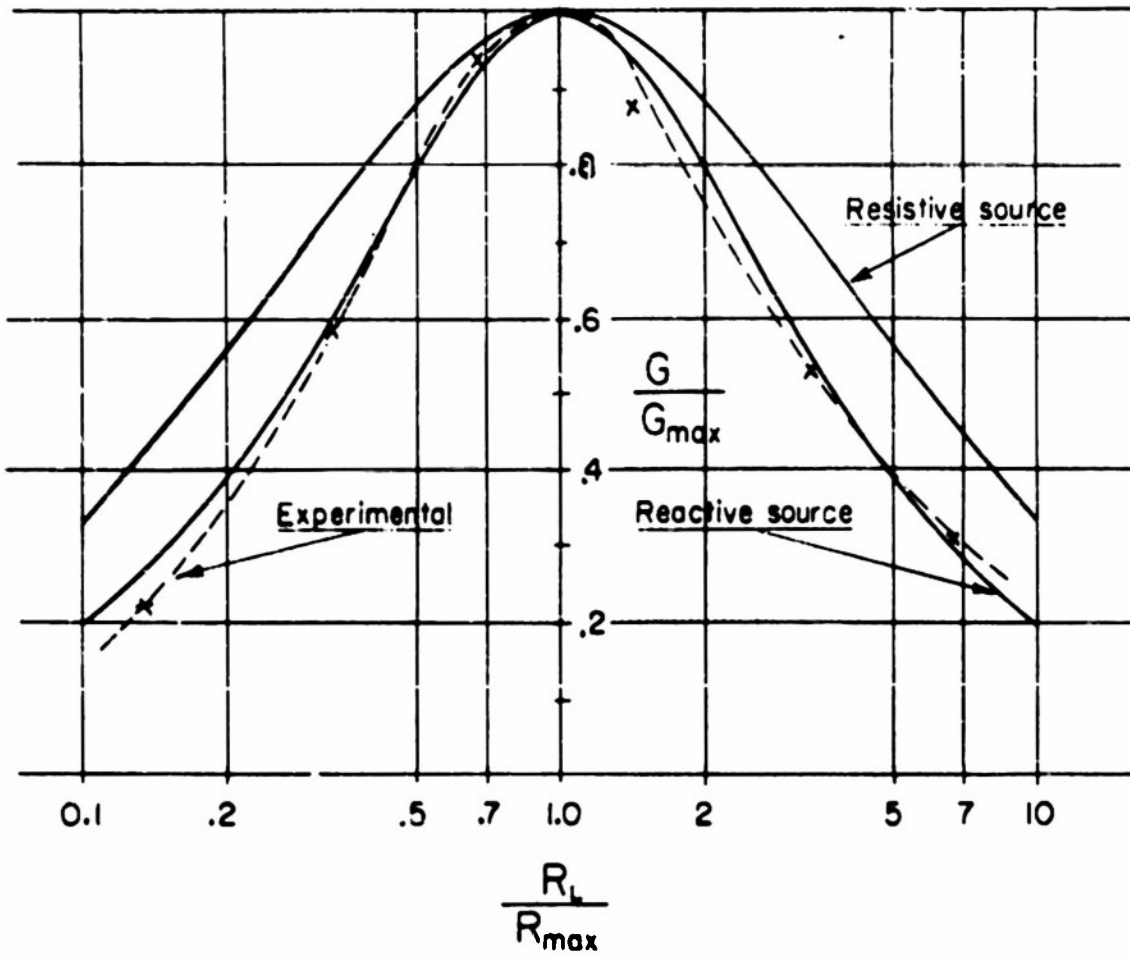
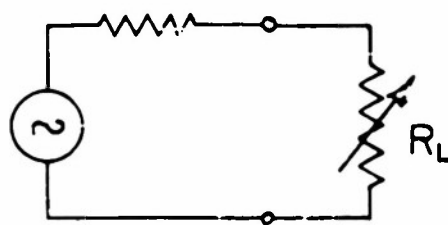


FIG. 3.12 Power Gain vs. Load Resistance



Reactive source



Resistive source

FIG. 3.13 Comparison of Power Transfer Curves

Reference to sections 2.6 and 2.8 will indicate that maximum power gain should occur when the load resistance is equal to the output winding reactance calculated at the second-harmonic frequency.

$$R_L(\text{for max. power gain}) = 2X_2 = 2(2\omega L) = 4\omega L \quad (48)$$

$$L = \frac{N_o^2 \mu_a A}{l} \frac{4\pi}{10} \times 10^{-8} \quad (28 \text{ repeated})$$

Using the experimentally determined value of μ_a and the measured physical parameters, Equation (28) yields:

$$L(\text{at } 600 \text{ cps}) = .168 \text{ mh.}$$

$$R_L(\text{for max. power gain}) = 4(2\pi \times 600)(.168) = 2540 \text{ ohms.}$$

Using the nominal measured value of L (≈ 75 mh):

$$R_L(\text{for max. power gain}) = 4(2\pi \times 600)(.075) = 1150 \text{ ohms.}$$

Fig. 3.12 indicates a value of $R_L = 1500$ ohms which is bracketed by the calculated values.

The value of maximum power gain is given by equation (42) repeated here for convenience:

$$G_{\text{max}} = \frac{8}{\pi} \frac{I}{R_w} \left(\frac{\mu_m}{\mu_a} \right)^2 f \quad (42 \text{ repeated})$$

Using the measured values of the parameters the theoretical power gain becomes:

$$G_{\max} = \frac{8}{\pi} \frac{.168}{0.72} \left(\frac{10 \times 10^4}{4 \times 10^4} \right)^2 600 = 2220 \text{ (using calculated value of L).}$$

$$G_{\max} = 990 \text{ (using nominal measured value of L).}$$

Fig. 3.12 indicates a value of $G_{\max} = 1400$ which is bracketed by the calculated values.

CHAPTER IV

CONCLUSIONS AND DESIGN CONSIDERATIONS

Several aspects of the analysis developed in Chapter II have been verified by the experimental work of Chapter III. The correlation between the analysis and the experiment is sufficiently high to allow the analysis to be used as a basis for design of second-harmonic magnetic modulators. Presented below are conclusions and design criteria based on the work of Chapters II and III and also the work of other experimenters in the field.

4.1 Choice of Modulator Configuration

Perhaps the simplest configuration consists of a single core wound with a sufficient number of windings to supply excitation, signal, and output requirements. The major disadvantage of such a configuration is the presence of large odd-harmonic components in the output winding. These components are usually much larger than the desired second-harmonic output signal and, unless selective circuits are used, there exists the possibility of overloading the stage following the modulator.

A much better configuration consists of two cores arranged so that the odd-harmonic components in each output winding cancel each other and hence do not appear in the output. The degree of odd-harmonic suppression depends on how well the magnetic characteristics of the two cores are matched. Normally two physically similar cores will be sufficiently well matched to give on the order of a 10 to 1 suppression of odd-harmonics. This can be improved by selecting matched cores or by adjusting the wind-

ings on each core to give the effect of matched cores. Differences in the width of the hysteresis loop can be minimized by altering the number of excitation turns in one or the other of the cores. Similarly, differences in maximum flux density can be minimized by altering output winding turns.

4.2 Choice of Excitation

A most important consideration in the choice of an excitation source is that it be able to supply sufficient mmf to saturate the core. In addition, the waveform of the excitation must be free from the harmonic component used as the output. To insure this, adequate filtering in the excitation circuit is necessary. Modulator transimpedance is a function of excitation amplitude; thus amplitude stability is important to prevent changes in gain.

Choice of excitation frequency depends on many factors. Output signal frequency and amplitude are directly dependent on excitation frequency; hence equipment following the modulator may dictate the choice.

The most important factors to be considered are indicated below.

Factors favoring choice of low excitation frequency:

- (1) Economy of excitation power
- (2) Core loss, and hence heating, is small
- (3) Impedance levels are lower
- (4) Freedom from winding resonances.

Factors favoring choice of high excitation frequency:

- (1) Larger gain
- (2) Faster time response thereby accommodating wider bandwidths of input signal.

It appears that high frequency operation is advantageous because of the large gains and speed of response available. This must be tempered with the fact that desirable magnetic properties are unfavorably altered with increases in frequency. Also, since frequencies are ultimately reached where excitation power increases at least as the square of frequency, temperature rise may well be the limiting factor.

4.3 Choice of Output

A system which uses the sum of all even harmonic components would utilize the maximum energy available as output. Such a system, however, detracts from the basic simplicity of the modulator by requiring wide-band amplification and demodulation schemes.

Single frequency output eliminates the above difficulties. Experimentally it has been found that the 4th and 6th harmonic amplitudes are smaller than the 2nd harmonic amplitude for a given signal. This, coupled with the fact that the second harmonic impedance is lower than that of the higher harmonics, tends to indicate that the second-harmonic component is most desirable as the output frequency.

4.4 Choice of Core

4.41 Core Material

Materials having high maximum permeability are best suited for use in magnetic modulators. Low core loss is important since it is desirable to operate the core at high frequencies without excessive heating. Thus a figure of merit for core materials operated at the upper end of their useful range can be defined as $\mu_m f_c$, where f_c is the frequency at which the core loss becomes appreciable.

Reference to section 2.7 indicates that an additional figure of merit for core materials might be μ_m/μ_a . Lack of time, however, has prevented experimental verification of its validity. In the event future experimentation shows that μ_m/μ_a is actually a valid figure of merit, an interesting conclusion can be drawn. A large value of μ_m/μ_a suggests the use of materials with wide, steep-sided hysteresis loops. Fig. 4.1 shows how the width of the hysteresis loop decreases μ_a and hence increases μ_m/μ_a .

The so-called "square-loop" materials have the desired characteristics and would appear useful as modulator cores on the basis of this figure of merit.

Listed below are the important properties of several materials which can be used in modulator construction.

<u>Material</u>	μ_m <u>gauss/oersted</u>	H_c (d-c) <u>oersted</u>	f_c <u>cps</u>	$\mu_m f_c$	<u>Remarks</u>
Transformer Irons	5×10^3	1.0	5×10^2	2.5×10^6	Values are for comparison purposes
4-79 Ni-Permalloy	10^5	0.05	10^4	10^9	Most practical in this application
Supermalloy	5×10^5	0.005	10^4	5×10^9	Very sensitive to mechanical shock
Deltamax	10^5	0.1	10^4	10^9	Grain-oriented; sensitive to mechanical shock
Ferrites	10^3	0.5	10^7	10^{10}	Structurally weak

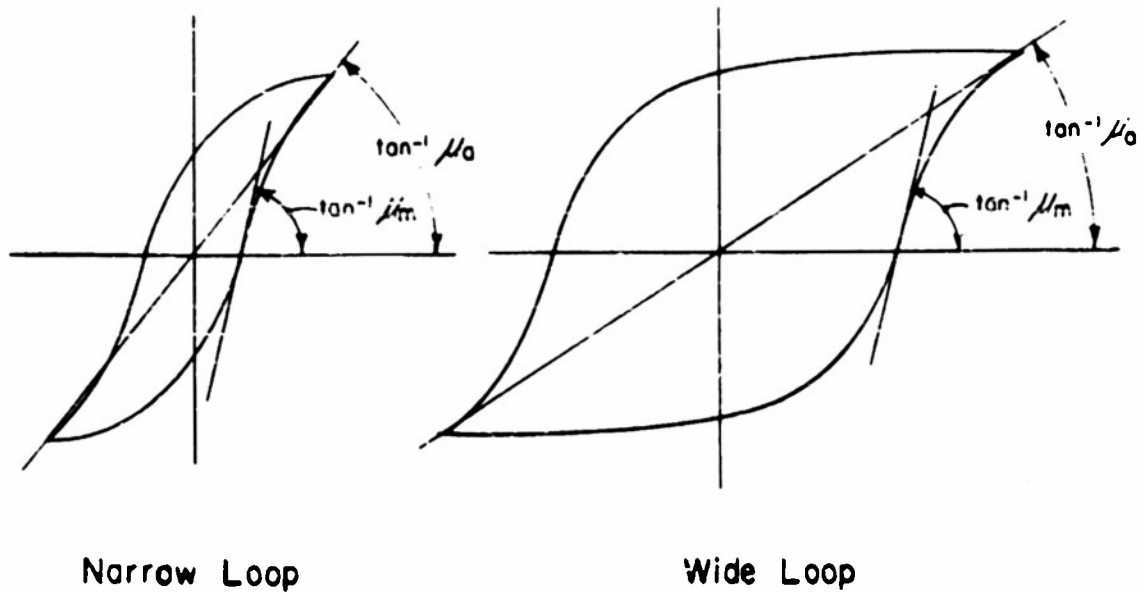


FIG. 4.1 Variation of $\frac{\mu_m}{\mu_a}$ with Width of Loop

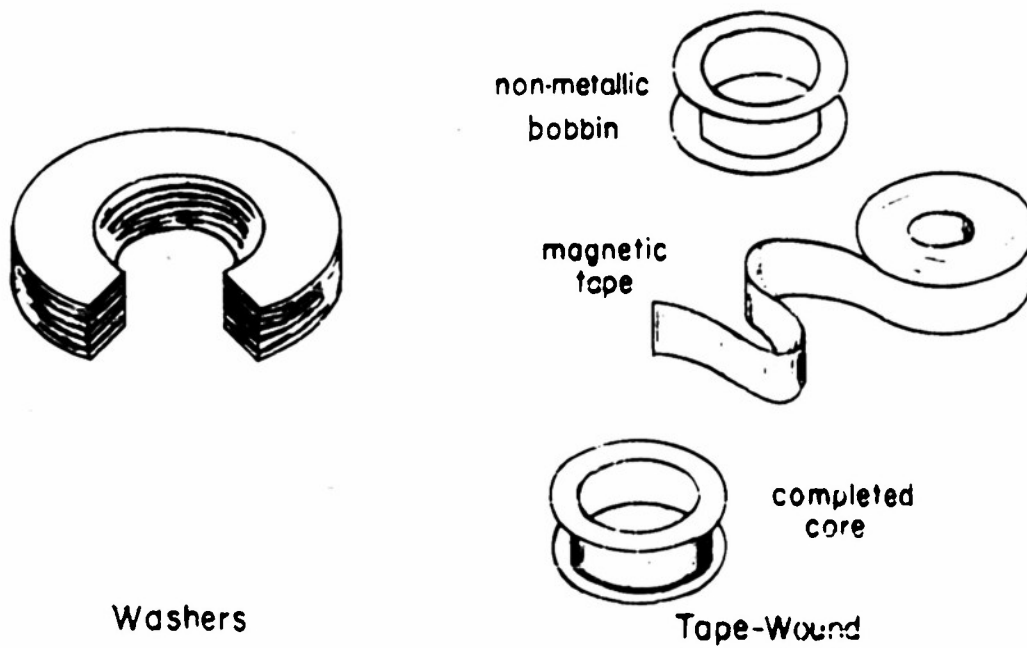


FIG. 4.2 Methods of Core Fabrication

4.42 Core Shape and Size

Since very high permeabilities are sought, air gaps must be eliminated. This suggests the use of toroidal cores. This type of core can be fabricated in either of two ways. Fig. 4.2(a) shows a core fabricated from washer-shaped stampings. This technique obviously cannot be used with grain-oriented materials. Fig. 4.2(b) illustrates a core fabricated by winding several turns of magnetic tape on a non-metallic bobbin.

In order to reduce core losses, lamination (or tape) thickness should be minimized. 1-mil tape is common, $\frac{1}{8}$ -mil tape is available, and thinner tapes are in prospect.

If a fixed volume is available for windings, both power output and time response depend directly on the ratio of core cross-sectional area to mean core length. Thus, the core size will depend on a compromise between the conflicting factors.

4.5 Windings

The excitation winding should take up as little of the available winding space as possible. Its wire size and number of turns will depend on the mmf required to saturate the core and the internal impedance of the excitation source. The winding should be distributed over the core so that the flux density is uniform across the area.

Separate windings for signal and output result in isolation between signal and output circuits but reduce sensitivity. Separate windings also allow impedance matching between signal source and modulator and modulator and load. The main advantage of a single winding used for both signal and output is the increase in sensitivity.

4.6 Circuits for Realizing Maximum Power Gains

The use of a single winding for both signal and output is not always compatible with impedance matching for maximum power transfer. Three techniques present themselves as solutions to this problem: (1) separate windings for signal and output, (2) the use of a transformer, and (3) "push-pull" arrangements. The choice among these methods depends on the impedances of the sources to be matched, and the relative frequencies of the signal and output.

The matching problem is fairly easy in the case of a high-impedance signal source and a load of somewhat lower impedance. Fig. 4.3 indicates two methods which can be used. A blocking capacitor for signal frequencies may be placed in series with R_L if signal and output frequencies are well separated and if winding resonances do not occur.

In Fig. 4.3 through Fig. 4.5 single-core modulators are shown for simplicity. However, the circuits are equally effective for two-core modulators which, as shown in section 2.8, offer the advantage of suppressing fundamental and odd-harmonic components.

As the signal source impedance becomes lower the matching problem becomes more difficult since the signal source tends to short-circuit the output winding. The use of a series load resistance, as shown in Fig. 4.4(a), is not effective because of the undesirable loss of signal power in R_L . The circuit of Fig. 4.4(b) employs a transformer which is used to present low impedance to signal frequencies and high impedance at the output frequency. The major difficulty of this circuit lies in the realization that the transformer itself may act as a modulator and introduce output components bearing no relation to the input signal.

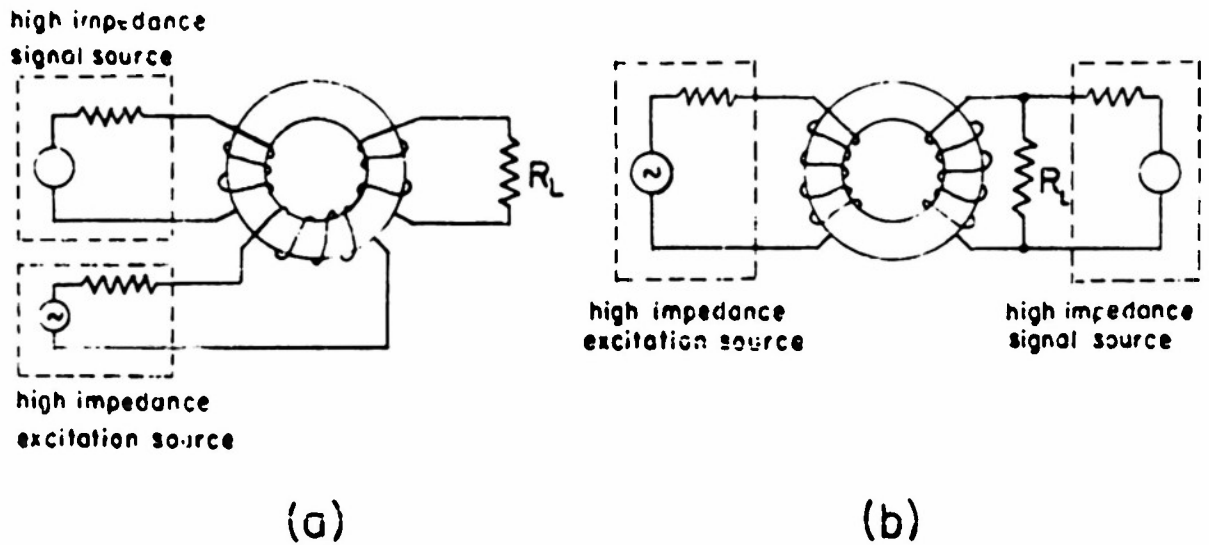


FIG. 4.3 Circuits used with High Impedance Signal Source

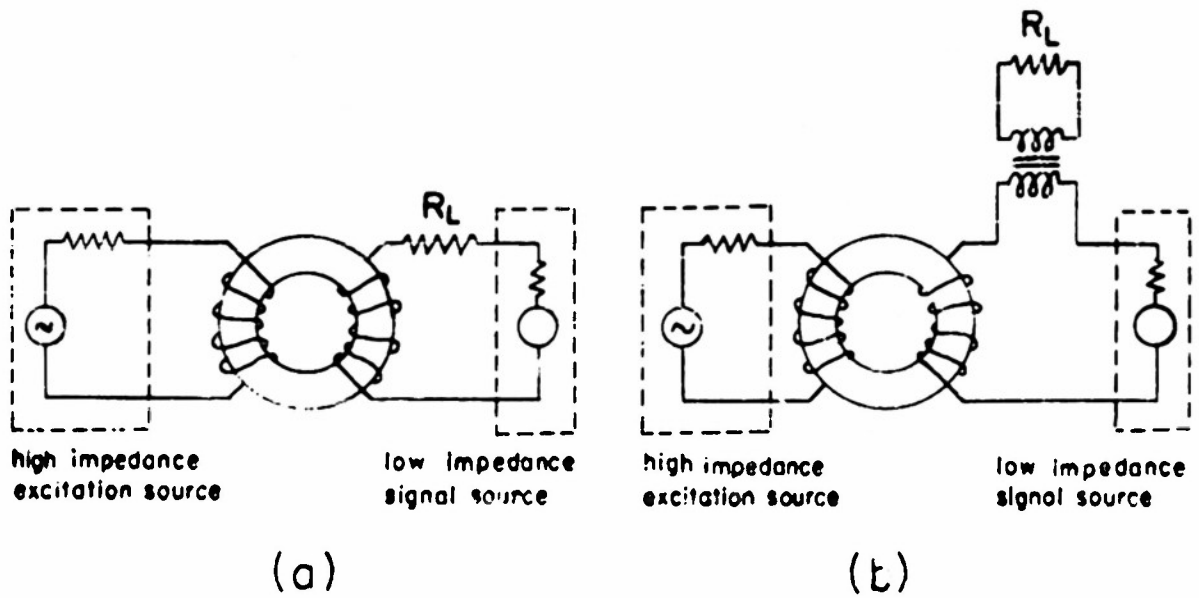
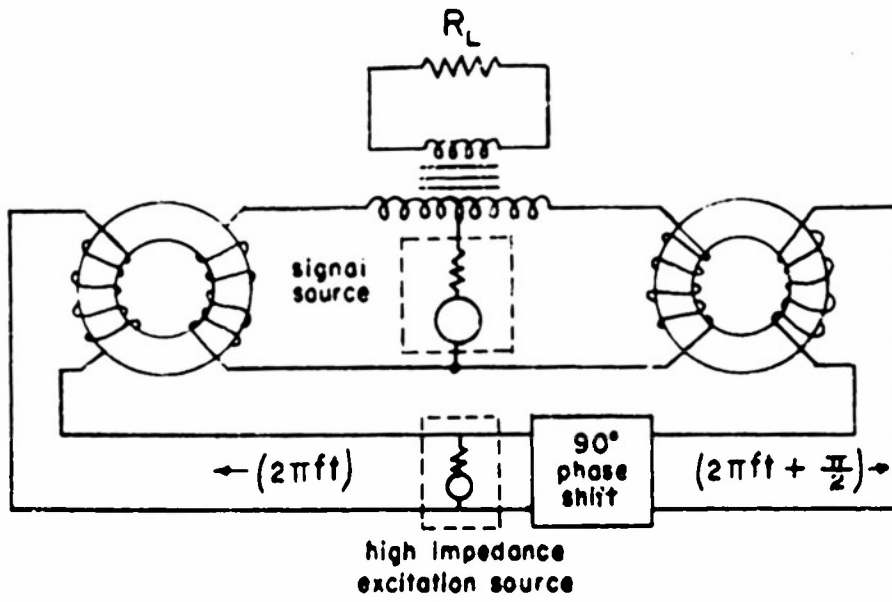
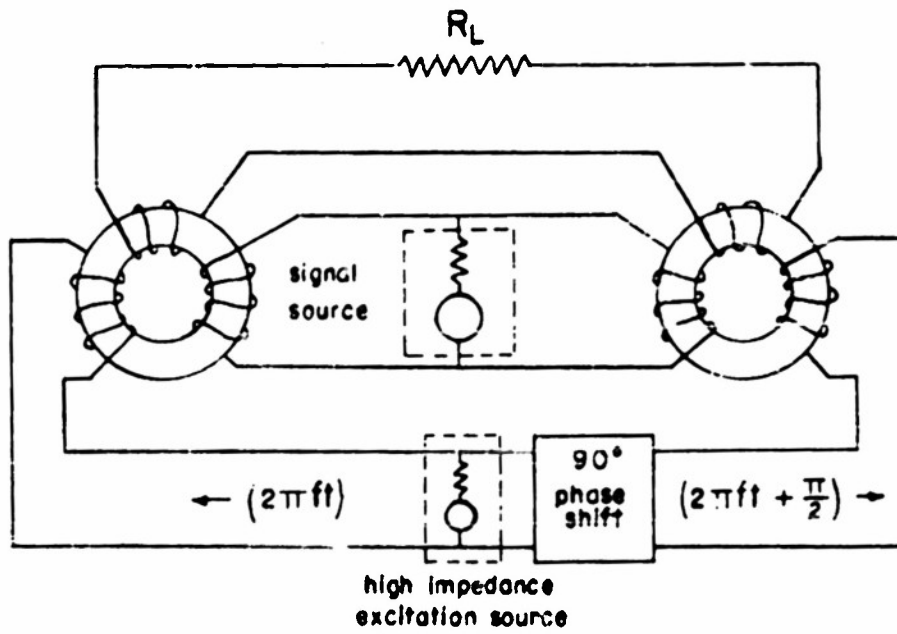


FIG. 4.4 Circuits used with Low Impedance Signal Source



(a)



(b)

FIG. 4.5 "Push Pull" Circuits

The "push-pull" circuit shown in Fig. 4.5(a) eliminates the non-linear difficulties of Fig. 4.4(b) by virtue of the inherent even-harmonic suppression of such a system. It is necessary that the excitation sources be 90° out of phase in order that the circuit act in a "push-pull" manner at the second-harmonic frequency. It should be noted that two reasonably well-matched magnetic modulators are necessary for this circuit to operate effectively. In addition, the dynamic characteristics of the center-tapped transformer must meet the same requirements as the transformer in Fig. 4.4(b).

A modified "push-pull" circuit which eliminates the need of an external transformer is shown in Fig. 4.5(b). Here the cores themselves act as the center-tapped transformer. Output is taken from a third set of windings on the core. Since these windings are isolated from the signal input windings, the output winding impedance does not affect the signal power delivered. By adjusting turns and wire size, the output winding impedance can be independently matched to the load R_L . This circuit still requires that the excitation sources be 90° out of phase.

CHAPTER V

WORK SUGGESTED BY THE PRESENT STUDY

In making this study several questions and avenues of investigation concerning the magnetic modulator have presented themselves. Lack of available time has, however, left these questions unanswered and the avenues untraveled. In the interests of completeness and also to indicate areas in which further investigation is necessary, some of the more pressing unknowns are here briefly discussed.

5.1 Behavior of Higher Output Harmonics

The relation between excitation amplitude and the amplitude of even-harmonics other than the second needs further investigation. Preliminary experimental investigation shows that these higher harmonics do not behave as predicted.

5.2 Threshold and Overload Signal Levels

No attempt has been made to carry operation of the modulator to either of these extremes. A study of methods by which the allowable range of input signals can be extended is needed. Although the expressions presented indicate what might be done to improve the input range, its implications should be considered. The use of feedback for improving linearity as well as dynamic range needs investigation.

5.3 Verification of μ_m/μ_a as a Figure of Merit for Core Materials

An experimental study should be made in order to determine the validity of this figure of merit. The study should consider the shape of the hysteresis loop and its relation to modulator gain and time response.

5.4 Voltage-Excited Modulator

An incomplete analysis has been made of a 2-core voltage-excited modulator. This analysis indicates that the open-circuit second harmonic output voltage depends on the same parameters found in the current-excited case. Preliminary experimental work indicates that this is actually the case.

The analysis needs to be developed and verified for other than open-circuit conditions so that analytic expressions for power gain and conditions for maximum power transfer can be formulated.

5.5 Determination of Frequency Response

Since the magnetic modulator is ideally suited to be used as an element in a closed-loop control system, it would be useful to express the operation of the device in the frequency domain and thus write its transfer function.

5.6 Power Measurement

The measurement of small electrical powers (1 milliwatt to 10 watts) over a wide frequency range presents the experimenter with a difficult task. This is especially true when the voltage and/or current is not sinusoidal, not necessarily in phase, and contains harmonics of high order. A device is sorely needed which will measure power of this character in the frequency range up to about 1 megacycle.

ACKNOWLEDGMENT

The author wishes to express his sincere appreciation to Professor Thomas F. Jones, Jr. for suggesting this problem, and for his guidance and criticism while the work was carried out.

He also wishes to thank Professor T.S. Gray, Professor A.B. Van Rennes, and the entire staff of the Electronic Nuclear Instrumentation Group of the Servomechanisms Laboratory of M.I.T. for their helpful suggestions and criticisms during the course of this work.

BIBLIOGRAPHY

1. The Arnold Engineering Co., Technical Data on Arnold Tape-Wound Cores, Bulletin TC-101A. Marengo, Illinois. March 1953.
2. A. Boyajian, "Mathematical Analysis of Non-Linear Circuits," General Electric Review, 34, 1931.
3. Electrical Engineering Staff of M. I. T., Magnetic Circuits and Transformers, New York, N.Y., John Wiley and Sons, Inc.
4. E.P. Felch, V.E. Legg, and F.G. Merrill, "Direct Current Amplifiers Employing Magnetrons," Bell Telephone Laboratories, Inc., Murray Hill, N.J., (advance copy, not released for publication.)
5. E.P. Felch, W.J. Means, T. Slonczewski, L.G. Parratt, L.H. Rumbaugh, and A.J. Tickner, "Airborne Magnetometers for Search and Survey," Trans. A.I.E.E., 66, (1947), 641--651.
6. A. Kusko, "Notes on the Magnetic Amplifier," M.I.T. Dept. of Electrical Engineering, Class Notes 2357, Dec. 6, 1951.
7. T.A. Ledward, "DC/AC Converter," Wireless World, Aug. 1943.
8. J.M. Manley, "Some General Properties of Magnetic Amplifiers," Proc. I.R.E., 39, (March 1951), 242--251.
9. S.W. Noble, and P.J. Baxandall, "The Design of a Practical D.C. Amplifier Based on the Second-Harmonic Type of Magnetic Modulator," Proc. I.E.E. Part II, 99, No. 70, (Aug. 1952).
10. G. Wennerberg, "A Simple Magnetic Modulator for Conversion of Millivolt D.C. Signals," Electrical Engineering, 70, (Feb. 1951), 144--147.
11. F.C. Williams and S.W. Noble, "The Fundamental Limitations of the Second-Harmonic Type of Magnetic Modulator as Applied to the Amplification of Small D.C. Signals," Proc. I.E.E. Part II, 97, No. 58, (Aug. 1950), 445--449.